AD-A069 194 ARNOLD ENGINEERING DEVELOPMENT CENTER ARNOLD AFS TN F/G 22/2
DATA VERIFICATION TESTS OF A 0.02-SCALE NASA SPACE SHUTTLE LAUN--ETC(U)
FEB 79 J A BLACK

UNCLASSIFIED AEDC-TSR-79-P7 NL

| OF |
AD
A069194

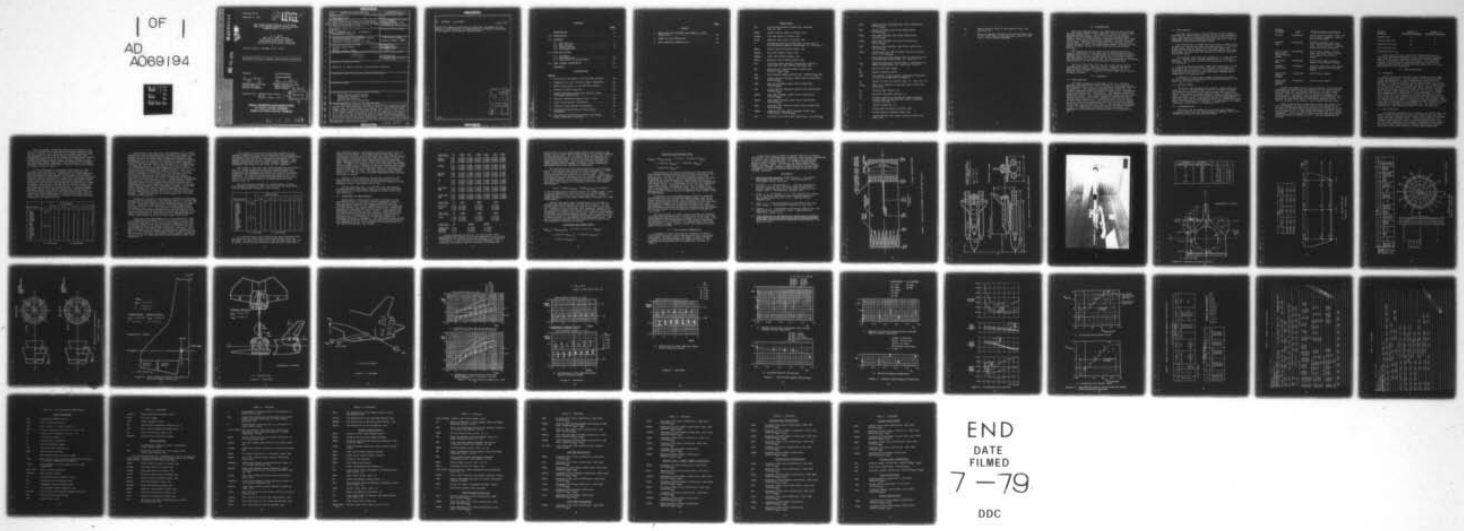

END
DATE
FILMED
7-79
DDC

AEDC-TSR-79-P7

February 5, 1979

LEVEL II

DATA VERIFICATION TESTS OF A 0.02-SCALE NASA SPACE SHUTTLE LAUNCH VEHICLE AT MACH NUMBERS FROM 0.60 TO 1.55

J. A. Black
ARO, Inc., AEDC Division
A Sverdrup Corporation Company
Propulsion Wind Tunnel Facility
Arnold Air Force Station, Tennessee

Period Covered: November 15-16, 1978

Approved for public release; distribution unlimited.

Reviewed By:

GREGORY COWLEY, 1st Lt, USAF
Test Director, PWT Division
Directorate of Test Operations

Approved for Publication:

FOR THE COMMANDER

JAMES D. SANDERS, Colonel, USAF
Director of Test Operations
Deputy for Operations

Prepared for: Johnson Space Center
EX 33
Houston, Texas 77058

ARNOLD ENGINEERING DEVELOPMENT CENTER
AIR FORCE SYSTEMS COMMAND
ARNOLD AIR FORCE STATION, TENNESSEE

REPORT DOCUMENTATION PAGE	READ INSTRUCTIONS BEFORE COMPLETING FORM
1. REPORT NUMBER: AEDC-TSR-79-P7	2. GOVT ACCESSION NO. / 3. RECIPIENT'S CATALOG NUMBER
4. TITLE (and Subtitle): Data Verification Tests of a 0.02-Scale NASA Space Shuttle Launch Vehicle at Mach Numbers from 0.60 to 1.55.	5. TYPE OF REPORT & PERIOD COVERED: Final Report, November 15-16, 1978
	6. PERFORMING ORG. REPORT NUMBER
7. AUTHOR(s): J. A. Black, ARO, Inc., a Sverdrup Corporation Company	8. CONTRACT OR GRANT NUMBER(s)
9. PERFORMING ORGANIZATION NAME AND ADDRESS: Arnold Engineering Development Center, Air Force Systems Command, Arnold Air Force Station, TN 37389	10. PROGRAM ELEMENT, PROJECT, TASK AREA & WORK UNIT NUMBERS: Program Element 921E01
11. CONTROLLING OFFICE NAME AND ADDRESS: Johnson Space Center, EX 33, Houston, Texas 77058	12. REPORT DATE: February 1979
	13. NUMBER OF PAGES: 46
14. MONITORING AGENCY NAME & ADDRESS (if different from Controlling Office)	15. SECURITY CLASS. (of this report): Unclassified
	15a. DECLASSIFICATION/DOWNGRADING SCHEDULE: N/A

16. DISTRIBUTION STATEMENT (of this Report)

Approved for public release; distribution unlimited.

17. DISTRIBUTION STATEMENT (of the abstract entered in Block 20, if different from Report)

18. SUPPLEMENTARY NOTES

19. KEY WORDS (Continue on reverse side if necessary and identify by block number)

Space Shuttle Launch Vehicle
Aerodynamic Characteristics
Angular Corrections
Wing Normal Force Corrections

20. ABSTRACT (Continue on reverse side if necessary and identify by block number)

A 0.02-scale model of the NASA Space Shuttle Integrated Launch Vehicle was tested November 15 and 16, 1978 in the Propulsion Wind Tunnel (16T) at free-stream Mach numbers from 0.60 to 1.55, free-stream dynamic pressures from 388 to 658 psf, angles of attack from -8 to 8 deg, angles of sideslip from -6 to 6 deg, and roll angles of 0, 180, -90, and 90 deg with nominal inboard elevon deflections of 10 deg and outboard elevon deflections of 5 deg. The objectives of the test were to determine applicable angular corrections in the

over

DD FORM 1 JAN 73 1473 EDITION OF 1 NOV 65 IS OBSOLETE

042550 LB

20. ABSTRACT (Concluded)

pitch and sideslip planes and to establish, throughout an α/β matrix, a data base for the determination of angular corrections to be applied to previously obtained data.

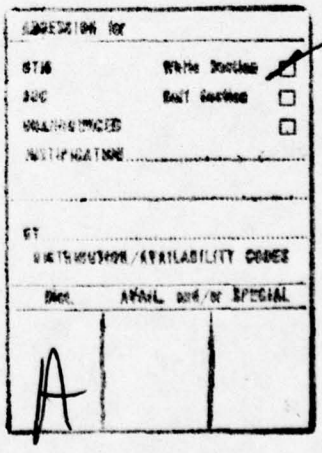

AFSC
Arnold AFS Tenn

CONTENTS

ILLUSTRATIONS

Page

TABLES

NOMENCLATURE

AFA	Pitch plane angular corrections, positive nose up, deg
ALFAL	Launch vehicle angle of attack, deg
ALFALS	Left SRB angle of attack, deg
ALFAT	External tank angle of attack, deg
b	Nondimensionalizing length used in calculation of wing bending moment coefficient, in. (see Fig. 5)
BETAL	Launch vehicle sideslip angle, deg
BETALS	Left SRB sideslip angle, deg
BETARS	Right SRB sideslip angle, deg
BETAT	External tank sideslip angle, deg
BFA	Crossflow plane angular corrections, positive from right to left looking upstream, deg
CBV	Vertical tail bending moment coefficient, moment/$Q(S_{REF})/\ell_{REF}$)
CBW	Wing bending moment coefficient, moment/$Q(S_{REF})$(b)
CNFL	Launch vehicle forebody normal force coefficient, force/$Q(S_{REF})$
CNFO	Orbiter forebody normal force coefficient, force/$Q(S_{REF})$
CNL	Launch vehicle measured normal force coefficient, force/$Q(S_{REF})$
CNFLS	Left SRB forebody normal force coefficient, force/$Q(S_{REF})$
CNFRS	Right SRB forebody normal force coefficient, force/$Q(S_{REF})$
CNFT	External tank forebody normal force coefficient, force/$Q(S_{REF})$
CNFTS	Combined ET plus SRB's forebody normal force coefficient, force/$Q(S_{REF})$
CSV	Vertical tail side force coefficient, force/$Q(S_{REF})$

CYFL	Launch vehicle forebody side force coefficient, force/$Q(S_{REF})$
CYFO	Orbiter forebody side force coefficient, force/$Q(S_{REF})$
CYFLS	Left SRB forebody side force coefficient, force/$Q(S_{REF})$
CYFRS	Right SRB forebody side force coefficient, force/$Q(S_{REF})$
CYFT	External tank forebody side force coefficient, force/$Q(S_{REF})$
CYFTS	Combined ET plus SRB forebody side force coefficient, force/$Q(S_{REF})$
$\bar{c}$	Nondimensionalizing length used in calculation of wing torsional coefficient, in. (see Fig. 5)
ℓ_{REF}	Nondimensionalizing length used in calculation of moment coefficients, in. (see Figs. 2 and 5)
M_∞	Free-stream Mach number
MRC	Moment reference center
PART	Part number (a data subset containing variations of only one independent parameter)
R_n	Radius on base of external tank, in. (see Fig. 4c)
X/C_{BF}	Ratio of a station on the body flap to the body flap chord
X_O	Orbiter body station, in.
X_T	External tank body station, in.
Y_O	Lateral station on the orbiter base, positive to the right of the vertical plane of symmetry looking upstream, in.
Z_O	Orbiter waterline, in.
α	Launch vehicle angle of attack, deg
β	Launch vehicle sideslip angle, deg
ϕ	Launch vehicle roll angle, positive right wing down, deg

ϕ_T	Radial angle on base of the external tank, deg (see Fig. 4c)
η	Ratio of spanwise station on the orbiter body flap to the total span of the body flap, positive from left to right looking upstream

1.0 INTRODUCTION

The work reported herein was sponsored by and conducted for the Johnson Space Center, NASA/JSC, Houston, Texas, under Program Element 921E01. The work was done at the Arnold Engineering Development Center, Air Force Systems Command (AFSC), Arnold Air Force Station, Tennessee by ARO, Inc., AEDC Division (a Sverdrup Corporation Company), contract operator of the AEDC. The test was conducted in the Propulsion Wind Tunnel Facility (PWT), Propulsion Wind Tunnel (16T) during the period November 15 and 16, 1978 under ARO Project Number P41T-B1.

The objectives of the test were to adequately define angular corrections in the pitch and sideslip planes at Mach numbers from 0.60 to 1.55 applicable to a 0.02-scale model of the NASA Space Shuttle Launch Vehicle and to provide a data base throughout an α/β matrix for the determination of angularity corrections to be applied to previously obtained data.

The final data from the test have been transmitted to Johnson Space Center, Houston, Texas. Requests for these data should be directed to Johnson Space Center, EX 33, Houston, Texas 77058. A copy of the final data is on file on microfilm at AEDC.

2.0 APPARATUS

2.1 TEST FACILITY

The AEDC Propulsion Wind Tunnel (16T) is a variable density, continuous-flow tunnel capable of being operated at Mach numbers from 0.2 to 1.6 and stagnation pressures from 120 to 4000 psfa. The maximum attainable Mach number can vary slightly depending upon the tunnel pressure ratio requirements with a particular test installation. The maximum stagnation pressure attainable is a function of Mach number and available electrical power. The tunnel stagnation temperature can be varied from about 80 to 160°F depending upon the available cooling water temperature. The test section is 16 ft square by 40 ft long and is enclosed by 60-deg inclined-hole perforated walls of six-percent porosity. The general arrangement of the test section with the test article installed is shown in Fig. 1. Additional information about the tunnel, its capabilities and operating characteristics is presented in Ref. 1.

2.2 TEST ARTICLE

The test article was a scaled replica of the Rockwell International Space Shuttle Vehicle in its launch configuration. The launch configuration consisted of the orbiter, an expendable external oxygen/hydrogen fuel tank (ET), and two expendable Solid Rocket Boosters (SRB's).

The orbiter has a blended wing body with a double delta planform (81 deg/45 deg) with full span elevons. The single, 45-deg swept vertical stabilizer had rudder deflection capability but was maintained at 0 deg throughout the tests. The single, aft body flap was present but was not deflected during the tests.

The external fuel tank was cylindrical in cross section having a tangent ogive forebody terminating in a biconic nose cap. The aft end of the ET was basically an ellipsoid of revolution.

The Solid Rocket Boosters (SRB) were attached to the ET by forward and aft attach lugs and were in the centerline horizontal plane of the ET. The SRB's were cylindrical in cross section and had an 18-deg semi-angle forebody which terminated in a spherical tip.

Dimensions of the primary model components are given in Fig. 2 and more detailed descriptions and drawings of the model may be found in Ref. 2.

2.3 SUPPORT SYSTEM

The Tunnel 16T standard sting support system which is shown in Fig. 1 and described in Ref. 1 was used to support and position the model in the test section during the test entry. The system utilized computer control to position the model at angles of attack and sideslip through combinations of pitch and roll angles. The support system is advantageous in that the model can be maintained close to the tunnel centerline where flow angularity is a minimum. A photograph of the model installed in the tunnel is presented in Fig. 3.

2.4 INSTRUMENTATION

The model was instrumented with strain-gage balances to measure individual and combined model component forces and moments utilizing the following balances:

Balance Location	Type	Measured Forces and Moments
Orbiter	6-component	Launch vehicle normal, side, and axial force; pitching, yawing, and rolling moment
External Tank	6-component	Combined external tank plus solid rocket boosters normal, side, and axial force; pitching, yawing, and rolling moment
Left & Right Hand Solid Rocket Booster (each)	6-component	Solid rocket booster normal, side, and axial force; pitching, yawing, and rolling moment
Left Hand Wing	3-component	Wing normal force, bending moment, and torsional moment
Vertical Stabilizer	3-component	Vertical stabilizer side force, bending moment and torsional moment
Right Hand Inboard Elevon	1-component	Elevon hinge moment
Right Hand Outboard Elevon	1-component	Elevon hinge moment

Forces and moments acting on the external tank alone were calculated by subtracting the summation of the forces and moments measured by the balances located in the solid rocket boosters from that measured by the balance located in the external tank. Similarly, orbiter forces and moments were calculated by subtracting those measured by the external tank balance (ET plus both SRB's), from those measured by the balance located in the orbiter (total launch vehicle loads).

Model pressures were measured by twelve individual pressure transducers located in the orbiter and external tank. In order to provide a good description of the pressure acting on the bases of the various model components, multiple pressure orifices were, in some instances, manifolded to a single transducer. The locations of these orifices and the pressure identifications are shown in Fig. 4, and are summarized as follows:

Orifice Location	Number of Manifold Pressures	Number of Measured Pressures
Orbiter base	9	3
Orbiter body flap	9	2
External tank base	45	5
Left hand SRB base	5	1
Right hand SRB base	5	1

Sting pitch and roll angles were determined from the outputs of synchro-transmitters and a strain gaged, pendulum type angle of attack indicator was mounted in the external tank as a redundant pitch angle indicator. The electrical signals from all position indicating devices, strain-gage balances, and pressure transducers were digitized for on-line data reduction and tabulation.

3.0 TEST DESCRIPTION

3.1 PROCEDURE

During testing the desired tunnel conditions were established and maintained. In the portion of the tests devoted to the determination of angle corrections, model angle of attack was varied at a nominal zero sideslip angle (ϕ = 0 and 180 deg), or model sideslip angle was varied at a nominal angle of attack of zero deg (ϕ = 90 and -90 deg). During testing of the α/β matrix, orbiter sideslip was varied from -6 to 6 deg at nominal constant angles of attack of -8 to 4 deg. Repeat runs, usually widely separated in time, were made to document data repeatability. The effects of load hysteresis in the pitch plane was investigated by pitching the model in a positive direction, then reversing the direction and pitching from the maximum positive angle of attack to the most negative angle of attack; acquiring data in approximate 2-deg increments. These tests may be identified in the Summary of Test Conditions by referring to the Model Attitude Schedules. All data were obtained at a unit Reynolds number of 3.0×10^6 per foot.

3.2 DATA REDUCTION

All measured pressures were converted into coefficient form. Those located on the orbiter base and orbiter body flap were used to correct measured normal force, axial force, and pitching moment for base pressure force. Pressures measured on the external tank base were used to correct measured axial force on that model component and pressures measured on the bases of the solid rocket boosters were used to correct both measured axial force and yawing moment on those model components.

Force and moment coefficient data were computed in the body axis coordinate system from the balances located in the orbiter, external tank, and both solid rocket boosters using the projection of the orbiter nose on the external tank longitudinal centerline as the moment reference point location. Forces and moments from the wing, vertical stabilizer, and elevons were computed about moment reference points unique to the individual model components. The location of the moment reference points and directions of positive forces and moments are shown in Figs. 2 and 5.

In the determination of angular corrections to apply to the data, many sources of information were available for analysis and consideration. Essentially all force components were considered as were several of the moment coefficients. Values of angular corrections in the pitch plane were extracted from the data by evaluation of normal force or bending moment coefficients obtained during pitch polars conducted at roll angles of 0 and 180 deg, and evaluation of side force or bending moment coefficients obtained during sideslip polars conducted at roll angles of -90 and 90 deg. In all instances, the coefficients were plotted against their respective model component angles of attack or sideslip for the evaluation. The listing below identifies the coefficients which were considered for the determination of pitch plane angular corrections, those that were actually utilized, and those that were eliminated from consideration:

Coefficient	ϕ	Mach Number				
		0.60	0.90	1.10	1.25	1.55
CNFL	0,180	U	U	U	U	U
CNFO	↓	U	U	U	U	U
CNFTS		U	U	U	U	U
CNFT		D	D	D	D	D
CNFLS		D	D	D	D	D
CNFRS		D	D	D	D	D
CNL		D	D	D	D	D
CBW	↓	U	U	U	U	U
CYFL	-90,90	U	U	U	U	-
CYFO	↓	U	U	U	U	-
CYFTS		U	U	U	U	-
CYFT		D	D	D	D	-
CYFLS		D	D	D	D	-
CYFRS		D	D	D	D	-
CSV		U	U	U	U	-
CBV	↓	D	D	D	D	-

U = Utilized D = Discarded

The external tank alone data and individual solid rocket booster data were eliminated from consideration because of the essentially articulating capability of the major model components relative to either their immediately adjacent model component or to the launch vehicle angle of attack or sideslip. As was mentioned in Section 2.4, each major model component (Orbiter, ET, and both SRB's) was mounted on, or suspended by, a 6-component balance. Of necessity, this type of model construction permitted each model component to pitch and yaw relative to its supporting or ground structure. This relative angular deflection phenomenon is shown in Fig. 6 for pitch polars conducted at roll angles of 0 and 180 deg, and sideslip polars conducted at roll angles of -90 and 90 deg. Included in these plots are angular differences determined under air-off conditions ($M_\infty = 0.0$). These angular differences were caused by balance deflections resulting from the model component weight and the weight distribution whereas those calculated from air-on conditions were the result of the same weight effects combined with aerodynamic loading. In general, tests conducted at 0 and 180 deg roll produced relative angular differences between either the ET and the Orbiter or the left SRB and the Orbiter of 0.25 to 0.30 deg at all Mach numbers. Right SRB data are not shown because of similarity to the left SRB results.

Figures 6c through 6e show angular differences determined between the ET and Orbiter, left SRB and Orbiter, and right SRB and Orbiter during sideslip polars conducted at $\phi = -90$ deg and 90 deg. These data show that only the ET retained the same position relative to the Orbiter at test Mach numbers that it assumed at $M_\infty = 0.0$. The positive β deflections relative to its static orientation indicated for the left SRB and the negative β deflections noted for the right SRB relative to its static orientation are reflective of the calculated SRB side forces which tended to force the SRB's away from the ET.

Since the prime requirement for a flow angularity probe, i.e., geometrical constancy at all roll angles, was violated by various components of the total launch vehicle model, the possibility exists that the coefficient differences utilized in the determination of angular corrections contain not only the effects of true tunnel flow angularity, but mutual interference effects and the effects of geometrical differences as well. It was therefore deemed appropriate to identify AFA and BFA only as pitch plane and sideslip plane angular corrections rather than by the more restrictive and definitive term "flow angularity."

Wing normal force data were discarded because of the apparent relatively large zero shifts which were indicated following tunnel shutdowns, and a relatively large normal force imprecision noted during the laboratory calibration of the balance and verified during in-tunnel check loadings. Wing bending coefficients were utilized, however, because of an acceptably high degree of precision in that component.

The values of AFA that were deemed acceptable are shown in Fig. 7a. These values were used in a computer curve fit routine and the resultant polynomials were evaluated both graphically and mathematically using the criteria of minimum residuals. The selected corrections are shown in Fig. 7b along with the angular corrections determined during earlier tests of a 0.03-scale model of the Space Shuttle Launch Vehicle (Ref. 3).

The coefficients analyzed for determination of cross flow angular corrections, BFA, are listed in the table below and are identified according to their usage:

Coefficient	ϕ	Mach Number				
		0.60	0.90	1.10	1.25	1.55
CYFL	0,180	U	U	U	U	U
CYFO	↓	U	U	U	U	U
CYFTS		U	U	U	U	D
CYFT		D	D	D	D	D
CYFLS		D	D	D	D	D
CYFRS		D	D	D	D	D
CSV		U	U	U	U	U
CBV	↓	U	U	U	U	-
CNFL	-90,90	U	U	U	U	-
CNFO	↓	D	D	D	D	-
CNFTS		D	D	D	D	-
CNFT		D	D	D	D	-
CNFLS		D	D	D	D	-
CNFRS		D	D	D	D	-
CBW	↓	U	U	U	U	-

U = Utilized D = Discarded

As indicated above, more coefficients were discarded from consideration for cross flow angular corrections than were utilized. At model roll angles of 0 and 180 deg, data from the ET alone, as well as data from the left and right hand SRB's

were discarded because of possible shielding effects from the adjacent ET or SRB's. The combined ET and SRB side force loading was utilized as were data from the total launch vehicle and orbiter alone because these loads were measured either on individual or combined model components having no adjacent model components which could shield them from possible crossflow. At model roll angles of -90 and 90 deg only total launch vehicle normal force coefficients and wing bending coefficients were utilized because at 90-deg roll angle, the orbiter would shield a portion of the ET and SRB's from any flow component coming from right to left. The same shielding effect would occur at ϕ = -90 deg if the crossflow components were directed from left to right.

Values of the acceptable coefficients utilized in the determination of the crossflow angular correction BFA are shown in Fig. 8a and the selected corrections along with those reported in Ref. 3 are shown in Fig. 8b.

The selected AFA (Fig. 7b) and BFA (Fig. 8b) angular corrections were vectorially added to the uncorrected model attitudes for all major model components during a post test data reduction.

3.3 UNCERTAINTY OF MEASUREMENTS

Uncertainties (bands which include 95 percent of the calibration data) of the basic tunnel parameters, shown in Fig. 10, were estimated from repeat calibrations of the instrumentation and from the repeatability and uniformity of the test section flow during tunnel calibration. Additional information concerning the uncertainties in the free-stream properties is discussed in Refs. 4 and 5. Uncertainties in the instrumentation systems were estimated from repeat calibrations of the systems against secondary standards whose uncertainties are traceable to the National Bureau of Standards calibration equipment. The instrument uncertainties are combined using the Taylor series method of error propagation described in Ref. 6 to determine the uncertainties of the reduced parameters shown below:

Type Load	M_∞	ΔCNF	ΔCY	ΔCAF	ΔCMF	ΔCLL	ΔCLN
Launch Vehicle	0.60	±0.0053	±0.0081	±0.0022	±0.0038	±0.0005	±0.0055
	0.90	±0.0039	±0.0060	±0.0016	±0.0028	±0.0004	±0.0041
	1.25	±0.0032	±0.0050	±0.0010	±0.0023	±0.0003	±0.0034
Orbiter	0.60	±0.0056	±0.0081	±0.0026	±0.0038	±0.0005	±0.0055
	0.90	±0.0042	±0.0060	±0.0020	±0.0028	±0.0004	±0.0041
	1.25	±0.0034	±0.0051	±0.0011	±0.0023	±0.0003	±0.0034
ET plus SRB's	0.60	±0.0019	±0.0009	±0.0015	±0.0006	±0.0002	±0.0002
	0.90	±0.0014	±0.0007	±0.0011	±0.0004	±0.0002	±0.0002
	1.25	±0.0012	±0.0005	±0.0006	±0.0003	±0.0001	±0.0001
ET	0.60	±0.0024	±0.0013	±0.0018	±0.0012	±0.0004	±0.0004
	0.90	±0.0018	±0.0009	±0.0013	±0.0008	±0.0003	±0.0003
	1.25	±0.0015	±0.0007	±0.0008	±0.0007	±0.0003	±0.0003
Left Hand SRB	0.60	±0.0010	±0.0007	±0.0007	±0.0007	±0.0003	±0.0005
	0.90	±0.0008	±0.0005	±0.0005	±0.0005	±0.0002	±0.0004
	1.25	±0.0006	±0.0004	±0.0004	±0.0004	±0.0002	±0.0003
Right Hand SRB	0.60	±0.0011	±0.0005	±0.0007	±0.0007	±0.0003	±0.0004
	0.90	±0.0008	±0.0004	±0.0005	±0.0005	±0.0002	±0.0003
	1.25	±0.0007	±0.0003	±0.0004	±0.0005	±0.0002	±0.0002

Type Load	M_∞	ΔCSV	ΔCBV	ΔCTV
Vertical Tail	0.60	±0.0030	±0.0026	±0.0013
	0.90	±0.0021	±0.0018	±0.0009
	1.25	±0.0017	±0.0015	±0.0008

Type Load	M_∞	ΔCNW	ΔCBW	ΔCTW
Wing	0.60	±0.0072	±0.0005	±0.0073
	0.90	±0.0054	±0.0004	±0.0054
	1.25	±0.0045	±0.0003	±0.0046

Type Load	M_∞	ΔCHEI	ΔCHEO
Inboard and Outboard Elevons	0.60	±0.0025	±0.0025
	0.90	±0.0019	±0.0019
	1.25	±0.0016	±0.0016

As was mentioned in Section 3.2, wing normal force measurements were deemed to be unsatisfactory for use in the determination of angular corrections because of unacceptably large errors in the calculation of that component. The laboratory calibration results indicated an uncertainty in

normal force of ±12.7 pounds when loaded on the axis of the balance and 13 pounds when loaded fore or aft (torsion loading) of the balance axis. The in-tunnel check loading also constituted an abbreviated calibration which was conducted at 5 load application points in both the positive and negative normal force direction. The results of these loadings produced maximum errors somewhat in excess of the uncertainty determined during the laboratory calibration.

The construction of the wing balance was a major contributor to the errors associated with the measurement of normal force. The balance was basically a short, thick, tang cantilevered from the left side of the fuselage. Because of the short span of the balance, the strain gages used to measure wing bending moment were spaced only 0.5532-in. apart (laboratory determination) in the spanwise direction. This distance was used in the equation to calculate force from two moment measurements;

$$\text{Force} = (\text{Moment}_{\text{inboard}} - \text{Moment}_{\text{outboard}})/d, \text{ where } d$$

is the aforementioned distance between the moment gages. Thus, it may be seen that an error on only 6 in.-lb in moment is converted into an error of 10.8-lb normal force. A much larger separation of the moment gages would obviously have been advantageous.

Several approaches were investigated in an attempt to improve upon the measurement of wing normal force: (1) all of the normal force errors were used in a curve fit routine as a function of the calculated (but erroneous) normal force; not considering whether the applied loads were increasing or decreasing, (2) normal force errors as a function of increasing or decreasing calculated bending moment, and (3) normal force errors as a function of decreasing calculated normal force and a second function of increasing calculated normal force. The latter approach produced the most satisfactory results with the correction functions as follows:

Increasing Wing Normal Force

$$F_{N_{Wing}} = F_{N_{Calculated}} - [2.1749 + 1.0174\text{-}01\ (F_{N_{Calc}}) + 1.0203\text{-}04\ (F_{N_{Calc}})^2 - 1.1805\text{-}06\ (F_{N_{Calc}})^3 - 1.1383\text{-}08\ (F_{N_{Calc}})^4]$$

Decreasing Wing Normal Force

$$F_{N_{Wing}} = F_{N_{Calculated}} - [-1.1917 + 1.1508\text{-}01\ (F_{N_{Calc}}) + 9.2311\text{-}05\ (F_{N_{Calc}})^2 - 1.5233\text{-}05\ (F_{N_{Calc}})^3 - 5.8816\text{-}09\ (F_{N_{Calc}})^4]$$

The ability of the above polynomials to fit the normal force errors determined during the in-tunnel calibration are shown in Fig. 10 over the calculated normal force range encountered in the test. Using the equations above, the error calculated by the polynomials was subtracted from the calculated normal force to produce a much closer relationship to true normal force. As illustrated in Fig. 10a for increasing wing normal force, a maximum error of ±3.0 lb could still remain in the data for negative loads, and as shown in Fig. 10b, a maximum error of ±2.4 lb could still be encountered at maximum positive force for polars conducted where normal force was decreasing.

In addition to the aforementioned correction functions, the outputs from the wing bending moment gages (from which normal force was calculated) were corrected for zero shifts which occurred during air-on testing periods by using the post-run zeroes to compute the previously obtained data. The uncertainties in the wing coefficients contain the effect of the correction functions but make no accounting for the effects of the zero shifts or the recomputation which corrected for zero shifts.

The uncertainties in model angle of attack and sideslip resulting from uncertainties in sting pitch, sting roll, and sting/balance deflections were estimated to be ±0.10 deg. The uncertainty in the determination of the angular corrections was estimated to be ±0.10 deg. In combined form, the final uncertainties in model angle of attack and sideslip are estimated to be ±0.14 deg.

4.0 DATA PACKAGE PRESENTATION

A summary of test conditions is presented in Table 1 correlating the type of data acquired with test Part number, Mach number, Reynolds number, and model attitude schedule. A sample of the tabulated data is shown in Table 2. The nomenclature associated with the tabulation is given in Table 3.

A copy of all data, either in tabular form or as a microfilm record, and including both corrected (flow angularity corrections included), and uncorrected model attitudes, was transmitted to the following organizations: (1) Rockwell International Space Division, Downey, California, (2) NASA-Johnson Space Center, Houston, Texas, and (3) Marshall Space Flight Center, Huntsville, Alabama. Magnetic tapes containing all data were transmitted to Chrysler Michoud Defense Space Division, New Orleans, Louisiana.

REFERENCES

1. Test Facilities Handbook (Tenth Edition). "Propulsion Wind Tunnel Facility, Vol. 4." Arnold Engineering Development Center, May 1974.

2. Daileda, J. J. and Marroquin, J. "Pretest Information for Test IA183 of the 0.02-Scale Model 89-OTS Space Shuttle Integrated Vehicle in the AEDC Propulsion Wind Tunnel (16T)." SD78-SH-0224, October 1978.

3. Black, J. A. and Graham, R. E. "Data Verification Tests of a 0.03-Scale NASA Space Shuttle Launch Vehicle at Mach Numbers from 0.60 to 1.55." AEDC-TSR-78-P54, November 1978.

4. Gunn, J. A. "Check Calibration of the AEDC 16-ft Transonic Tunnel." AEDC-TR-66-80 (AD633277), May 1966.

5. Jackson, F. M. "Supplemental Calibration Results for the AEDC Propulsion Wind Tunnel (16T)." AEDC-TR-70-163 (AD872475), August 1970.

6. ICRPG Handbook for Estimating the Uncertainty in Measurements Made with Liquid Propellant Rocket Engine Systems. Interagency Chemical Rocket Propulsion Group CPIA No. 180, April 30, 1969.

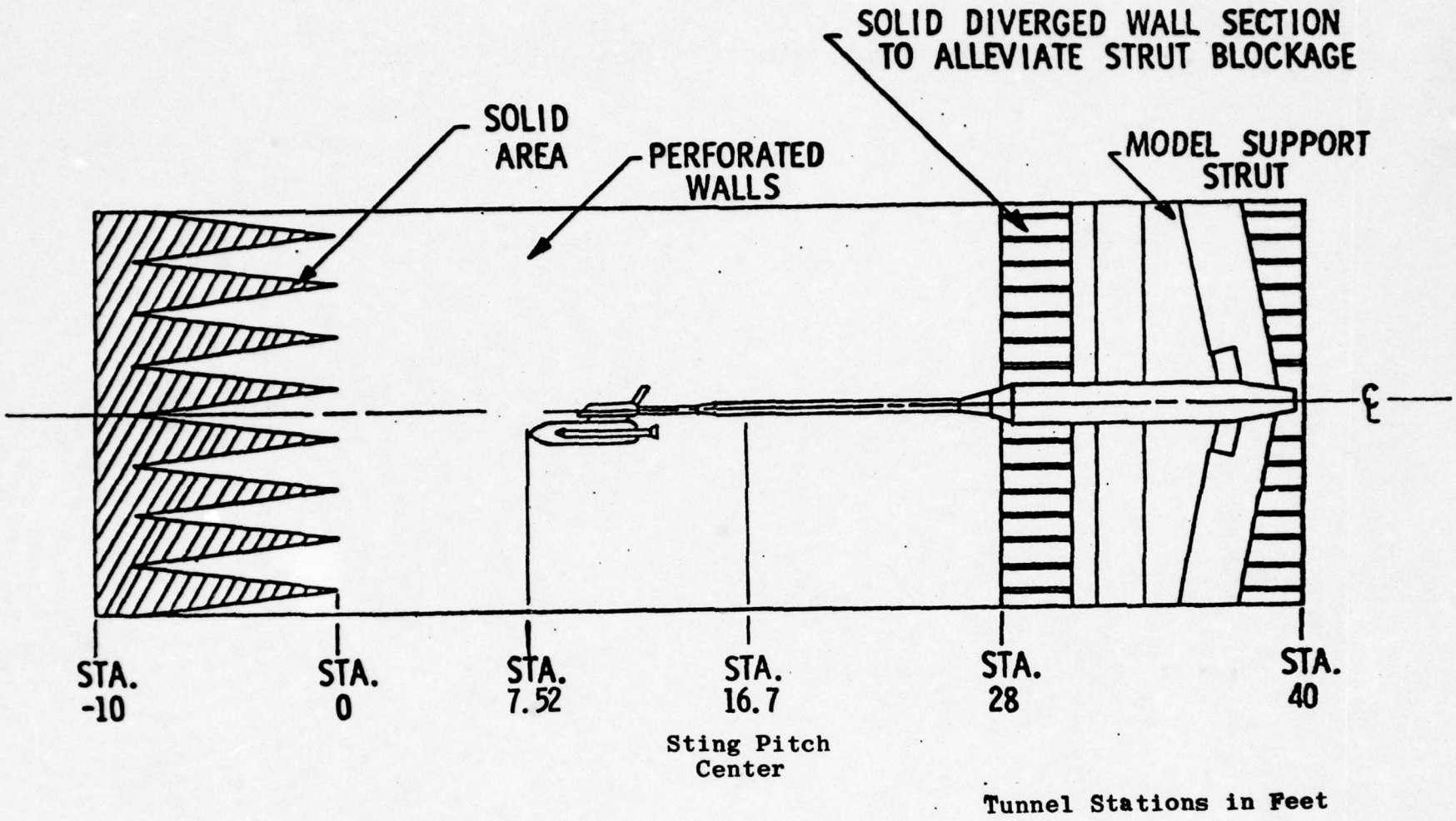

Figure 1. Location of the Model in the 16T Test Section

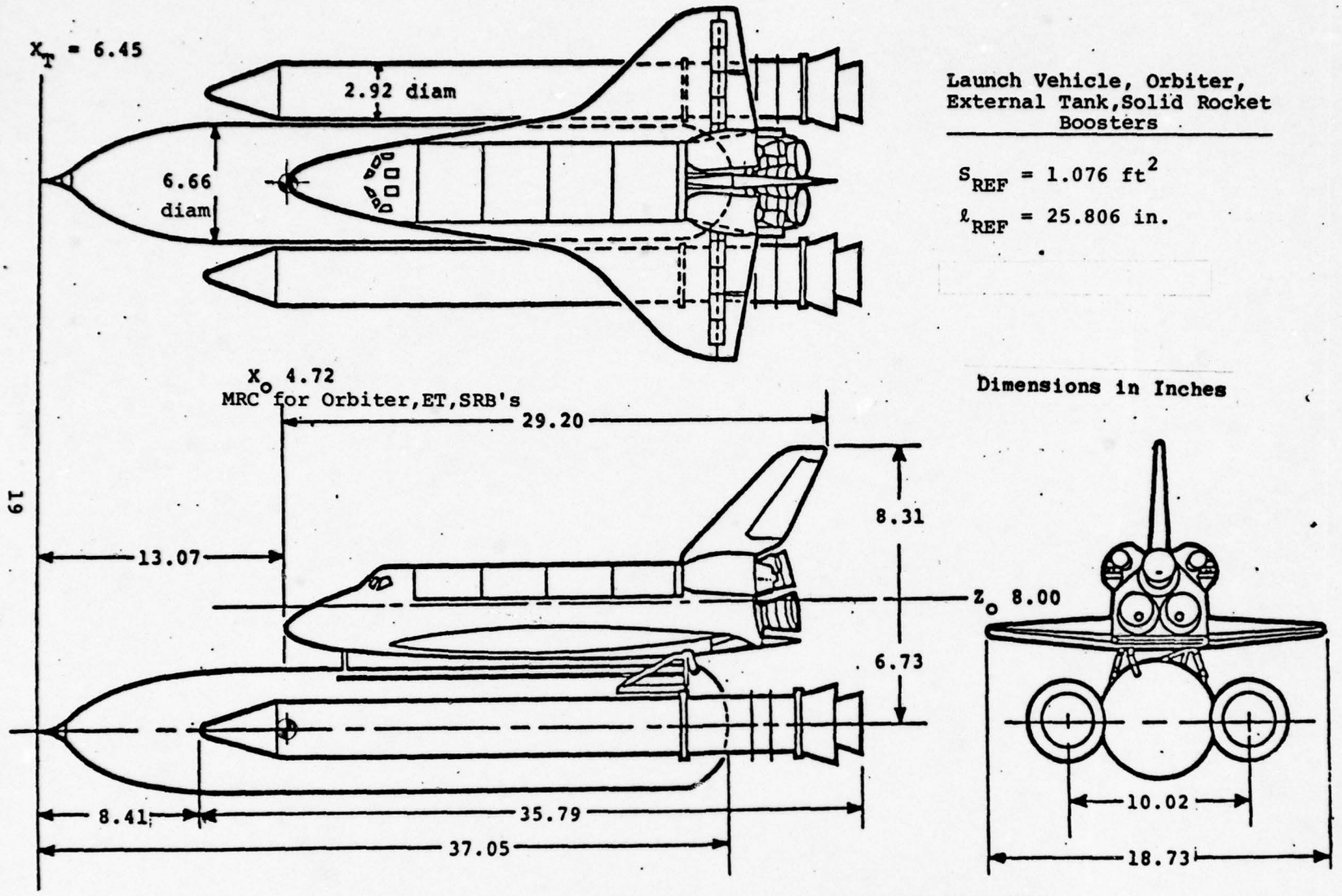

Figure 2. Dimensions of the 0.02-Scale Model Components

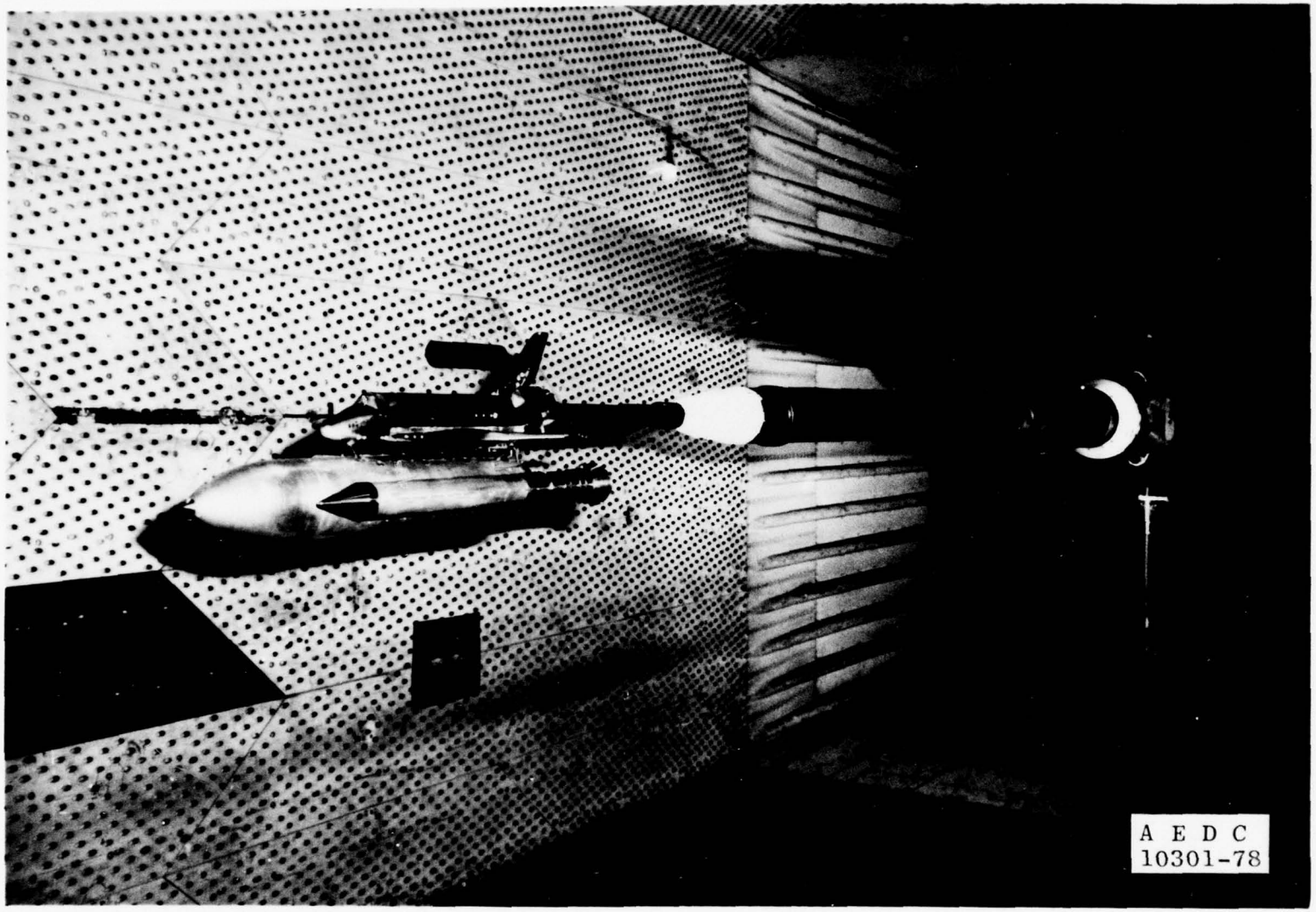

Figure 3. Model Installation in the 16T Test Section

Pressure Identification	Orifice Identification	Z_o	Y_o
302	302	10.1	0.0
↓	306	6.04	0.0
	312	8.78	-1.56
	316	7.52	-2.06
	318	6.04	-2.06
319	319	10.28	-1.10
↓	321	10.44	-2.06
	323	8.78	-2.14
325	325	Cavity	0.0

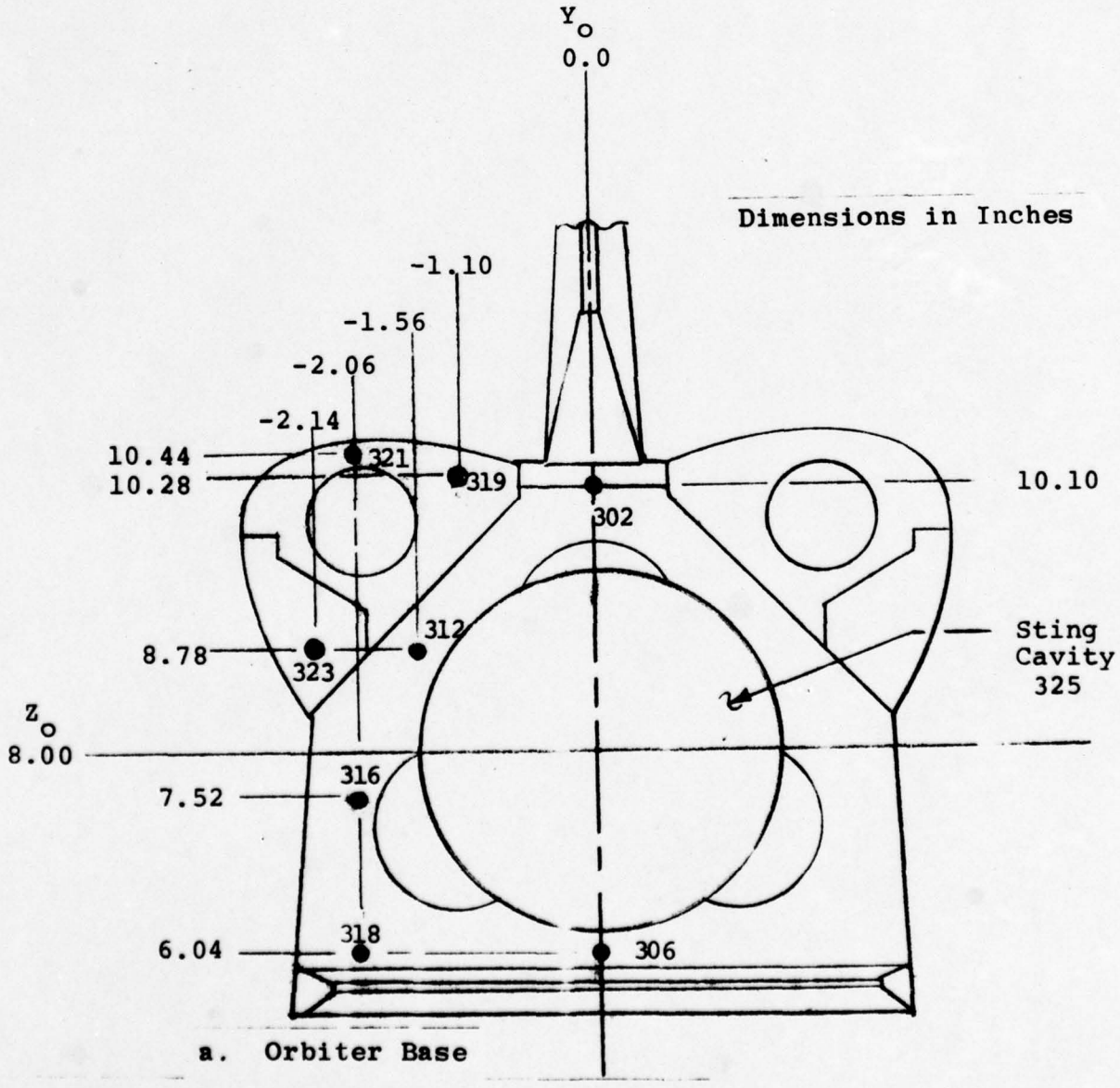

a. Orbiter Base

Figure 4. Pressure Orifice Locations

η	X/C_{BF}			Pressure Ident.
	-0.10	0.60	0.95	
0.10	405	407	408	405
0.50	413	415	416	413
0.90	437	439	440	405

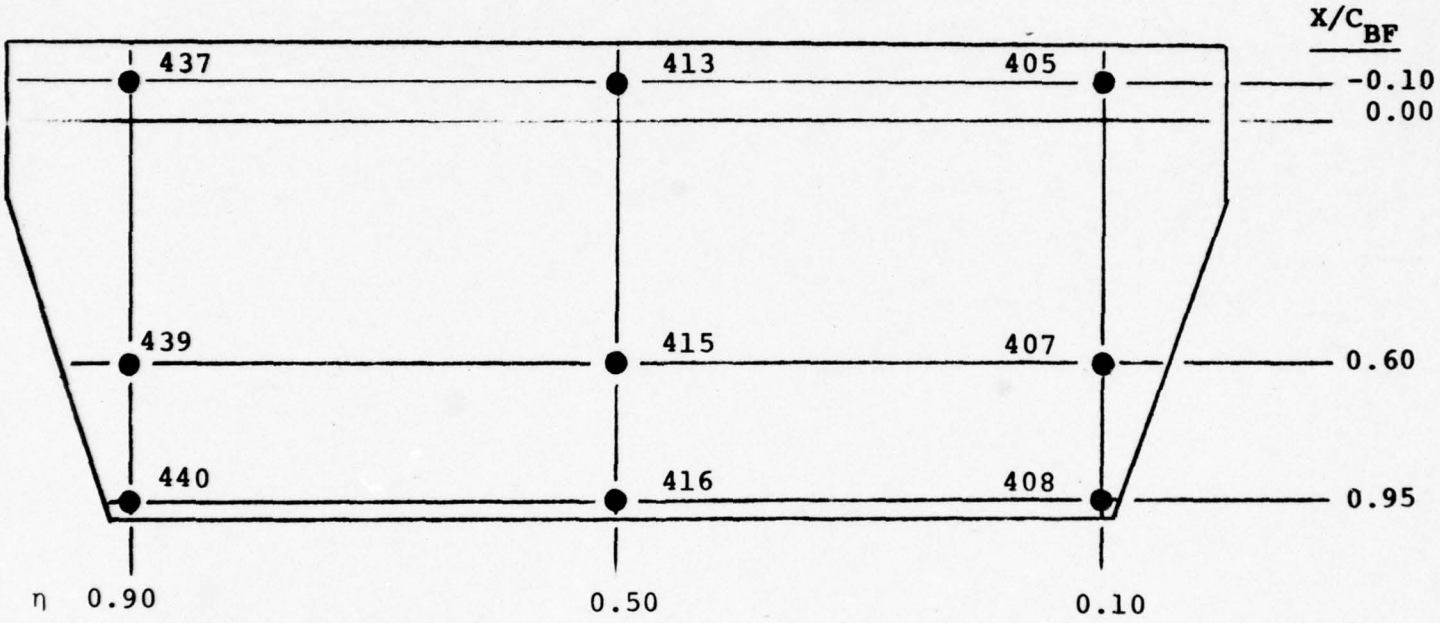

b. Orbiter Body Flap

Figure 4. Continued

Radius Model Scale	ϕ_T deg 0	15	30	45	60	90	1125	135	157.5	180	202.5	225	247.5	270	300	Pressure Ident.
3.13	1502		1503	1501	1504	1505	1506	1507		1509		1511	1512	1513	1514	1501
2.96	1516		1517		1518	1519	1520	1521		1523		1525	1526	1527	1528	1516
2.78	1530	1531		1533	1534	1535	1536	1537	1538	1539	1540	1541		1543	1544	1530
2.10	1546					1549		1551		1553		1555		1557		1546
1.55						1563								1571		1546
0	1574															1574

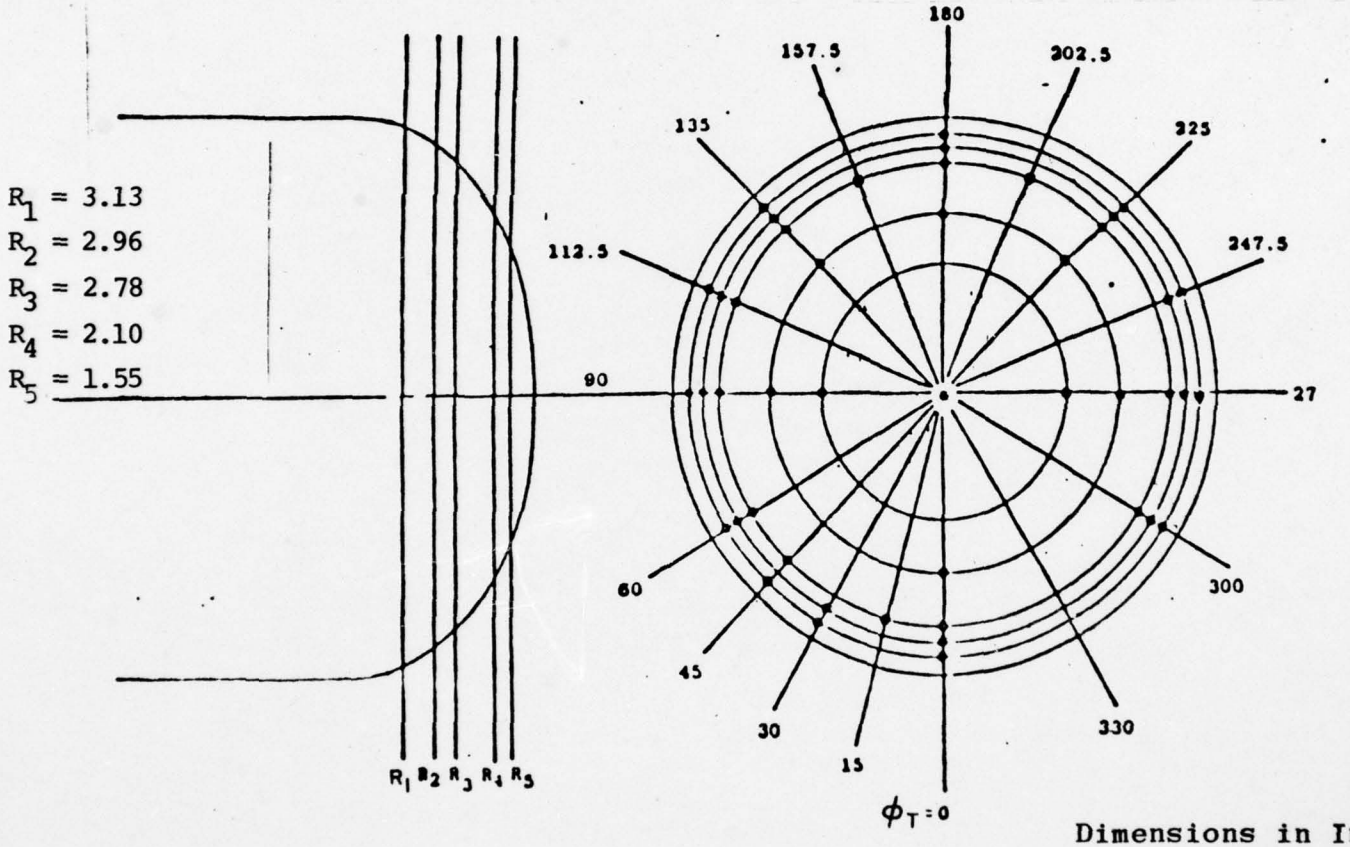

Dimensions in Inches

c. External Tank Base

Figure 4. Continued

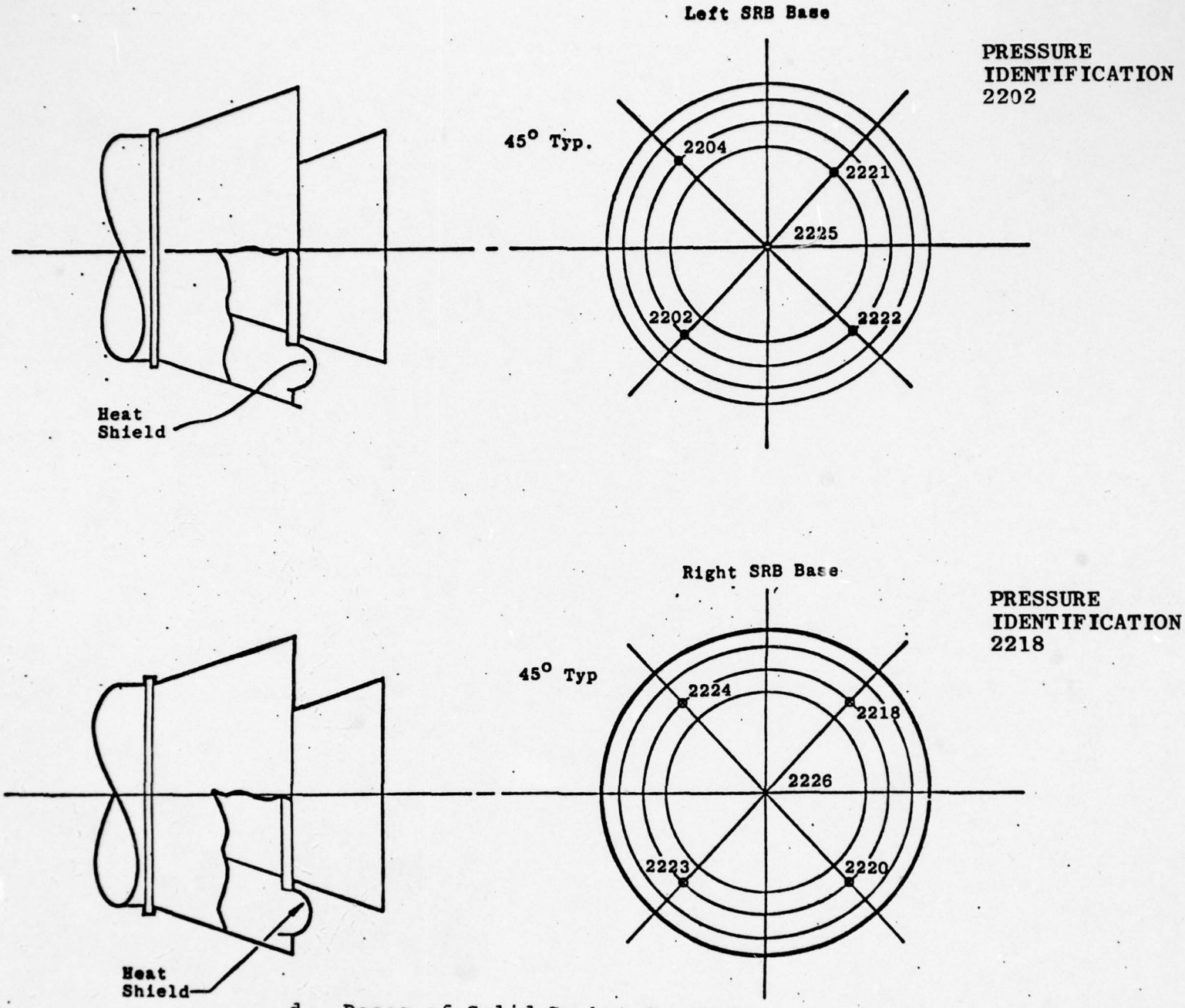

d. Bases of Solid Rocket Boosters

Figure 4. Concluded

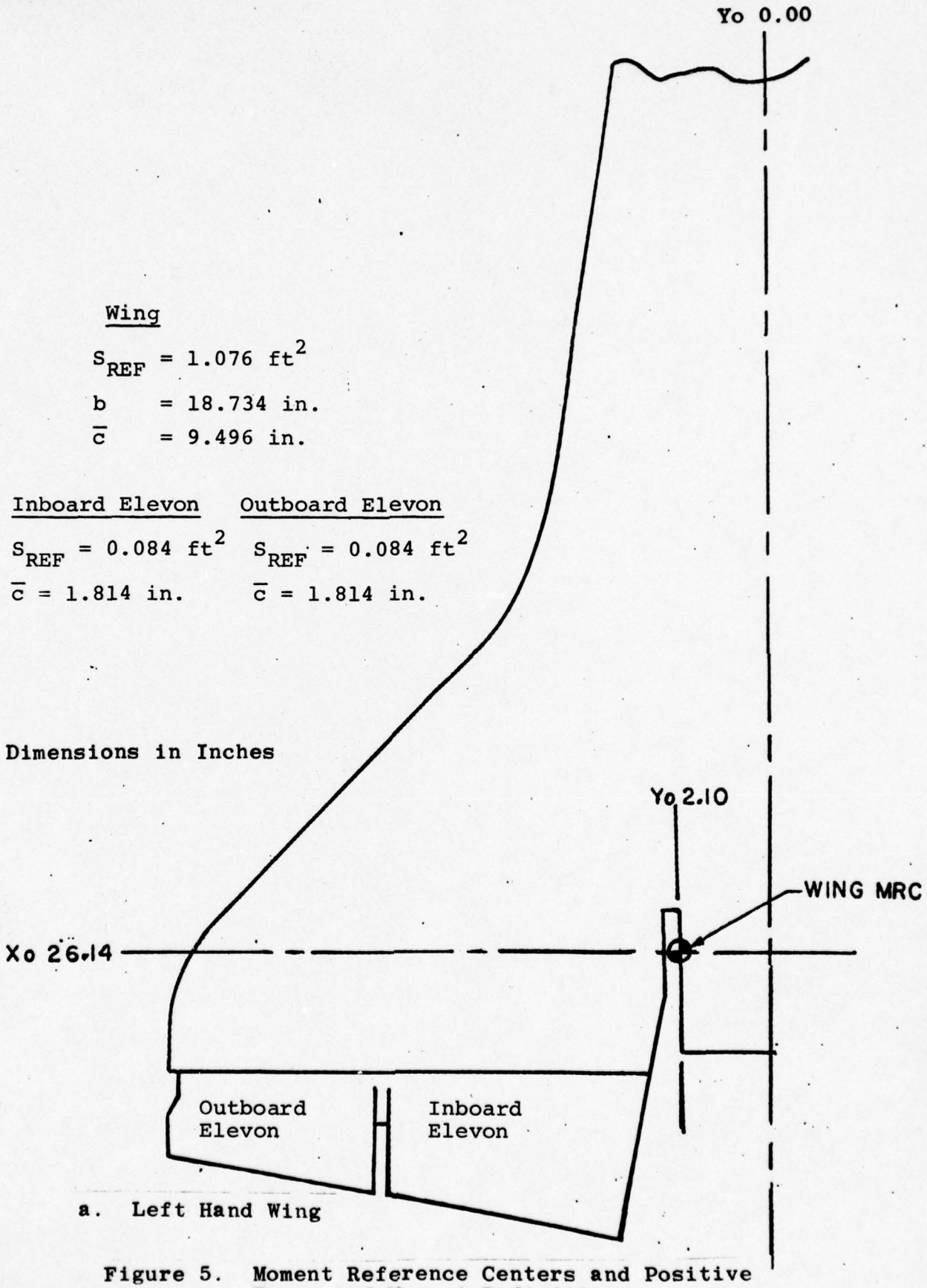

Figure 5. Moment Reference Centers and Positive Force and Moment Definitions

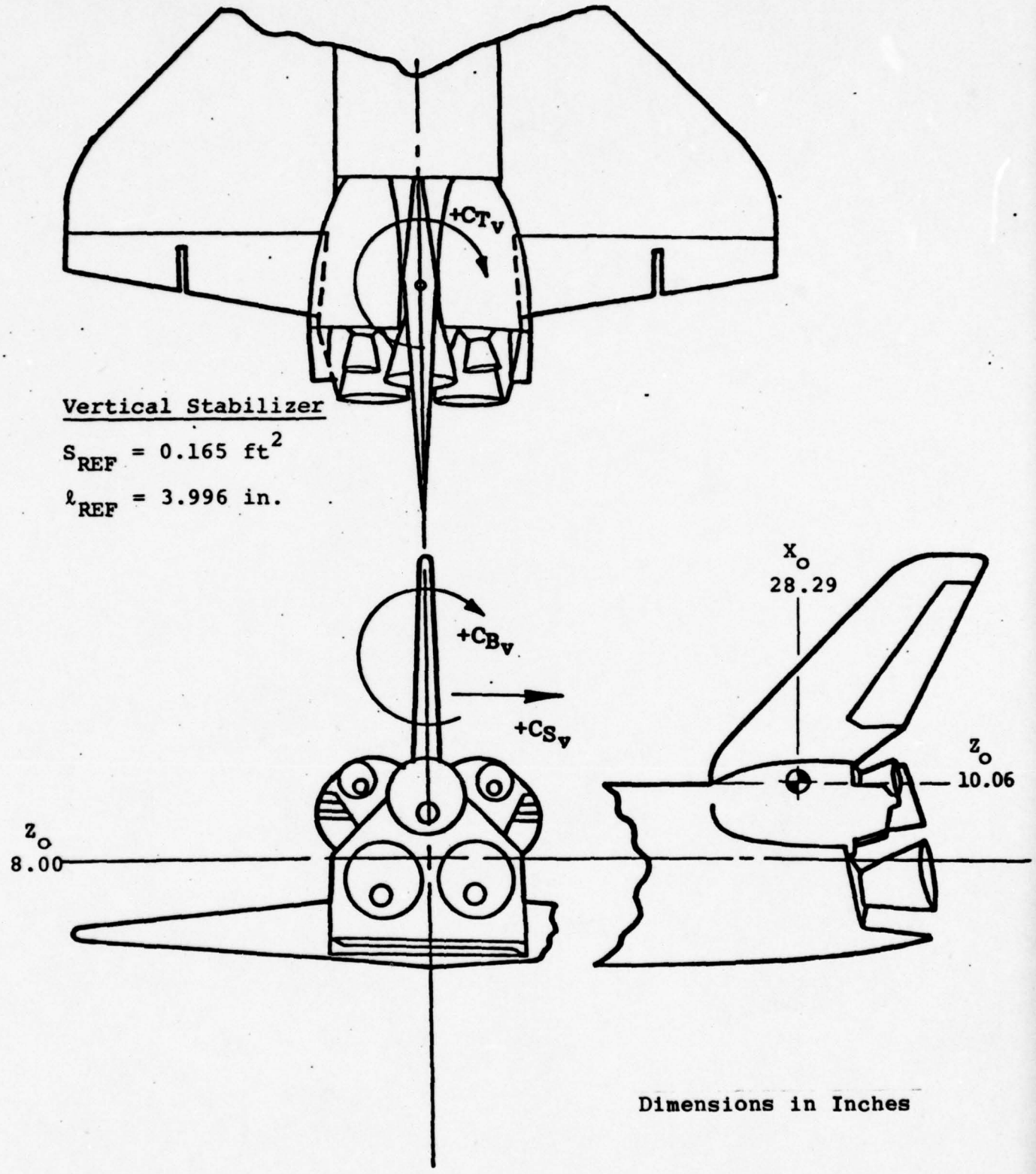

b. Vertical Tail

Figure 5. Continued

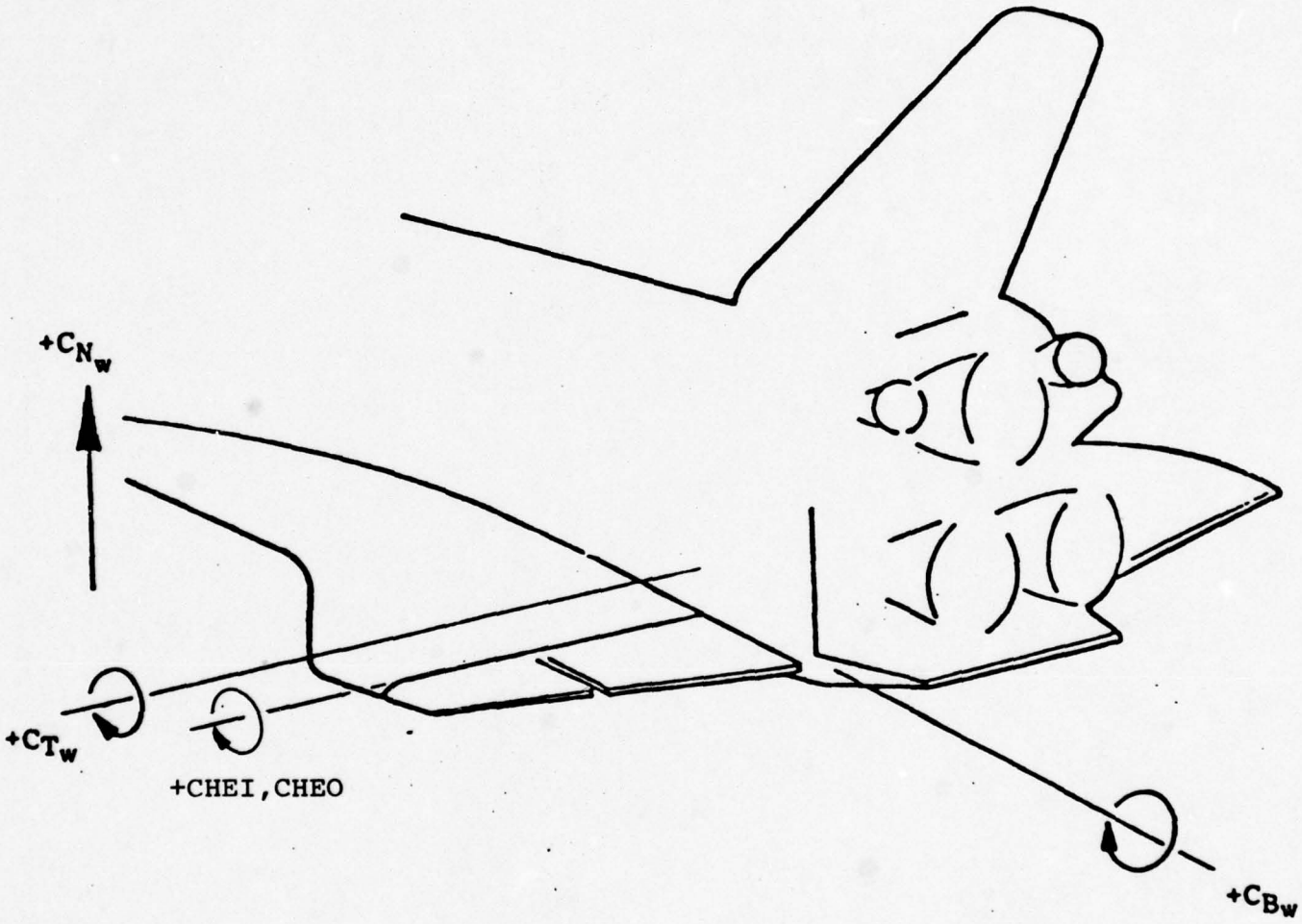

c. Wing and Elevons

Figure 5. Concluded

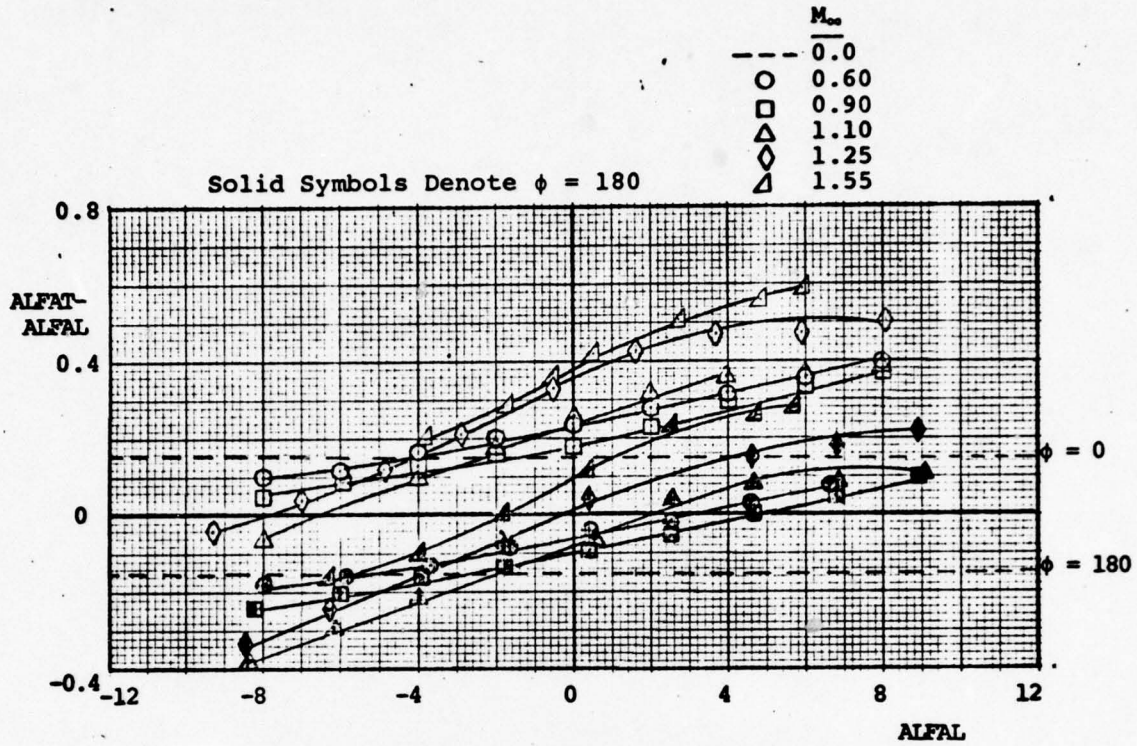

a. Differences in Launch Vehicle and External Tank Angles of Attack at 0 and 180 deg Roll Angles

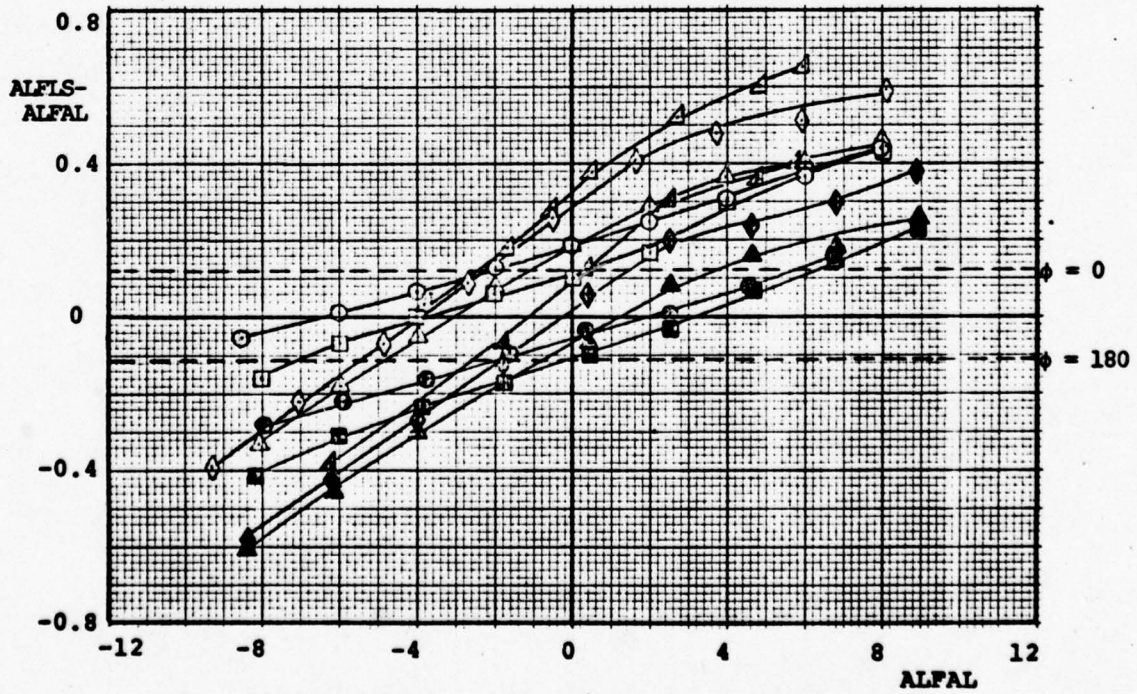

b. Differences in Launch Vehicle and Left Solid Rocket Booster Angles of Attack at 0 and 180-deg Roll Angles

Figure 6. Relative Deflection Angles at M_∞ = 0.90

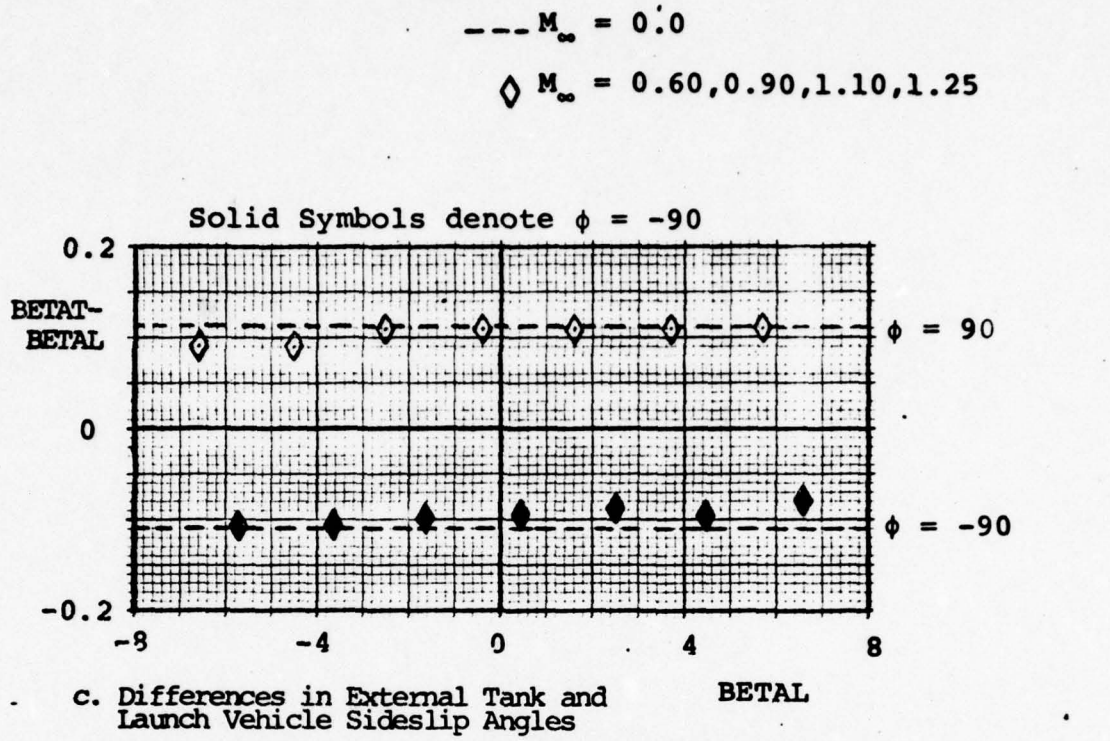

c. Differences in External Tank and Launch Vehicle Sideslip Angles

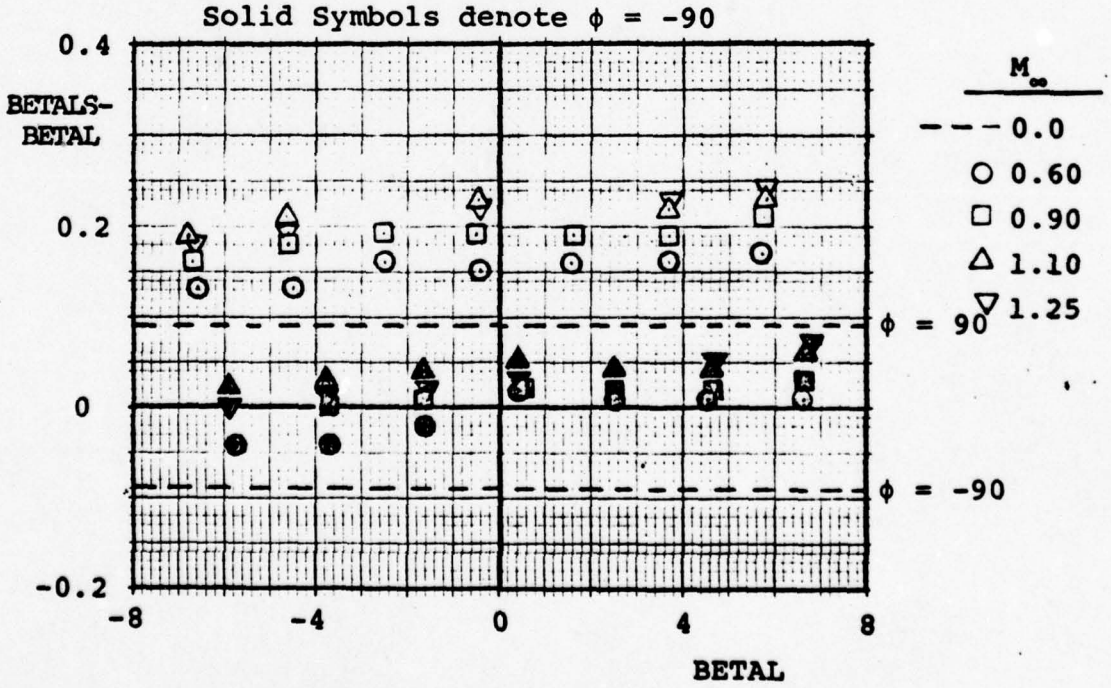

d. Differences in Left SRB and Launch Vehicle Sideslip Angles

Figure 6. Continued

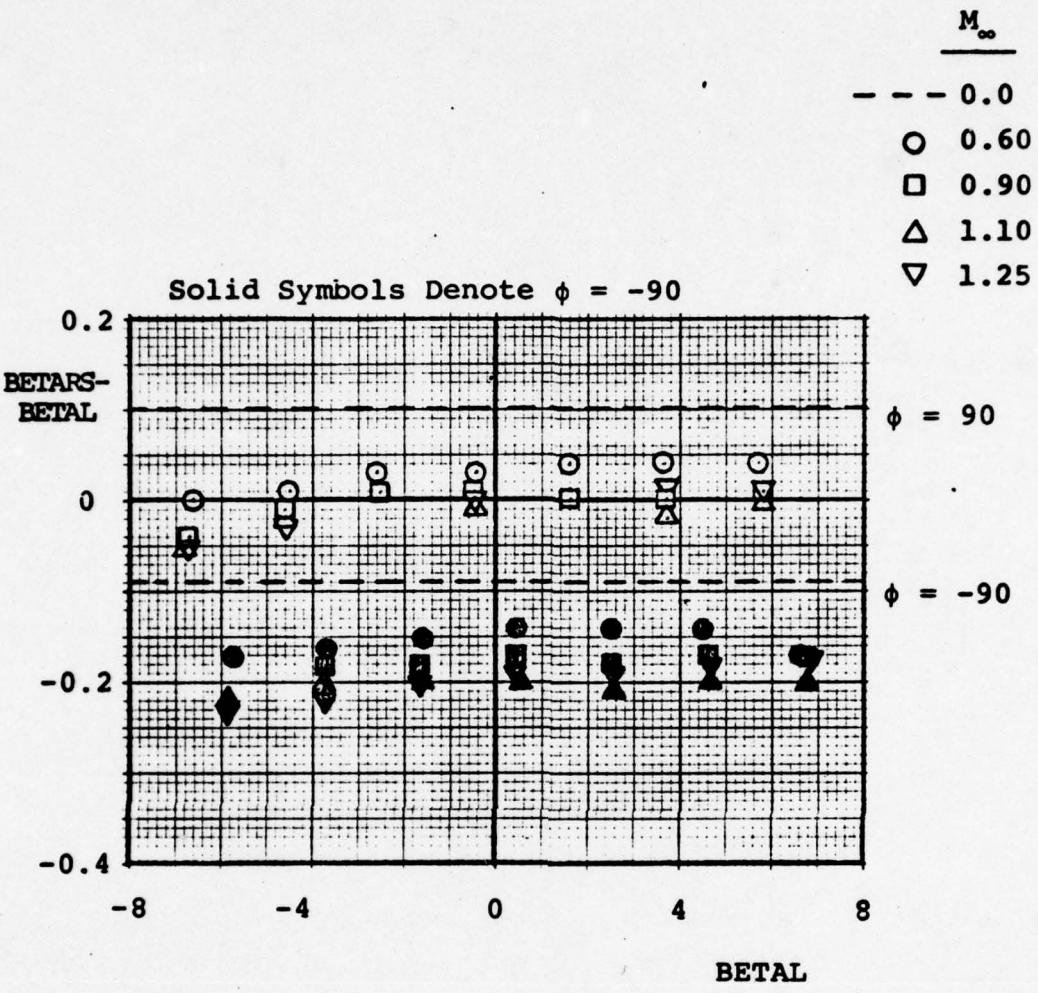

e. Differences in Right SRB and Launch Vehicle Sideslip Angles

Figure 6. Concluded

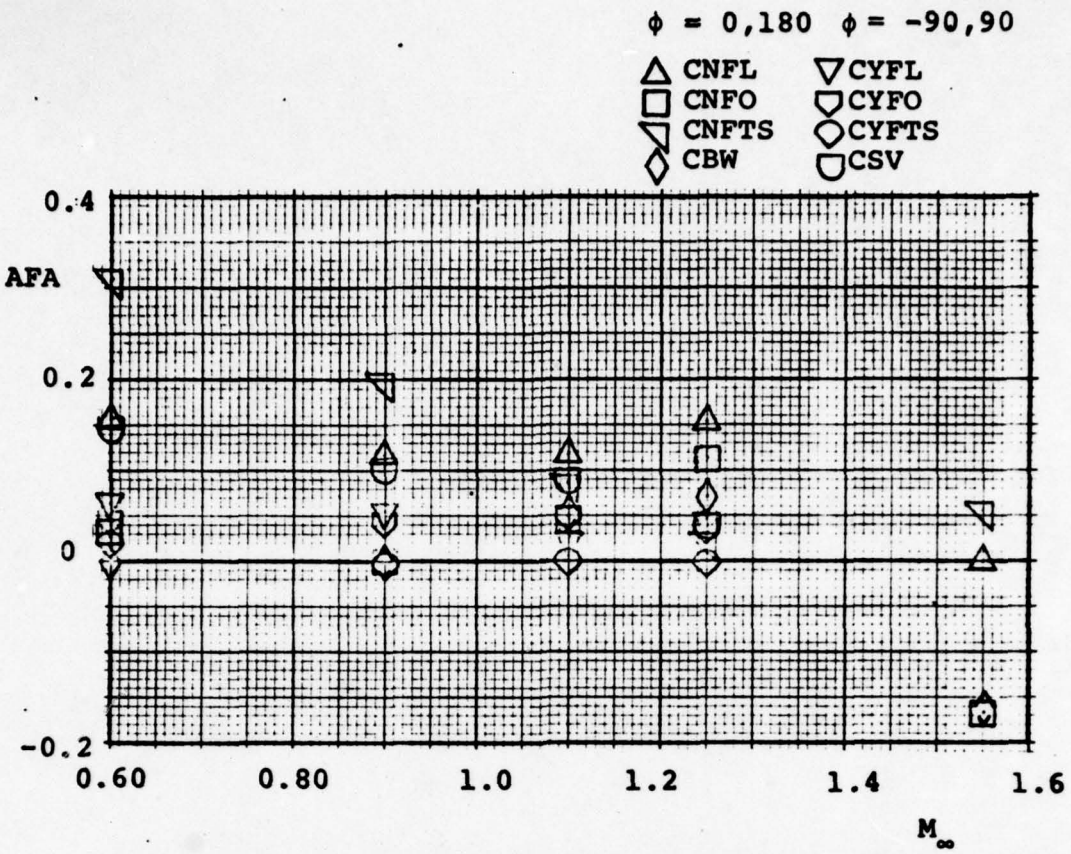

a. Angular Corrections Determined from 180-deg Opposed Balance Components

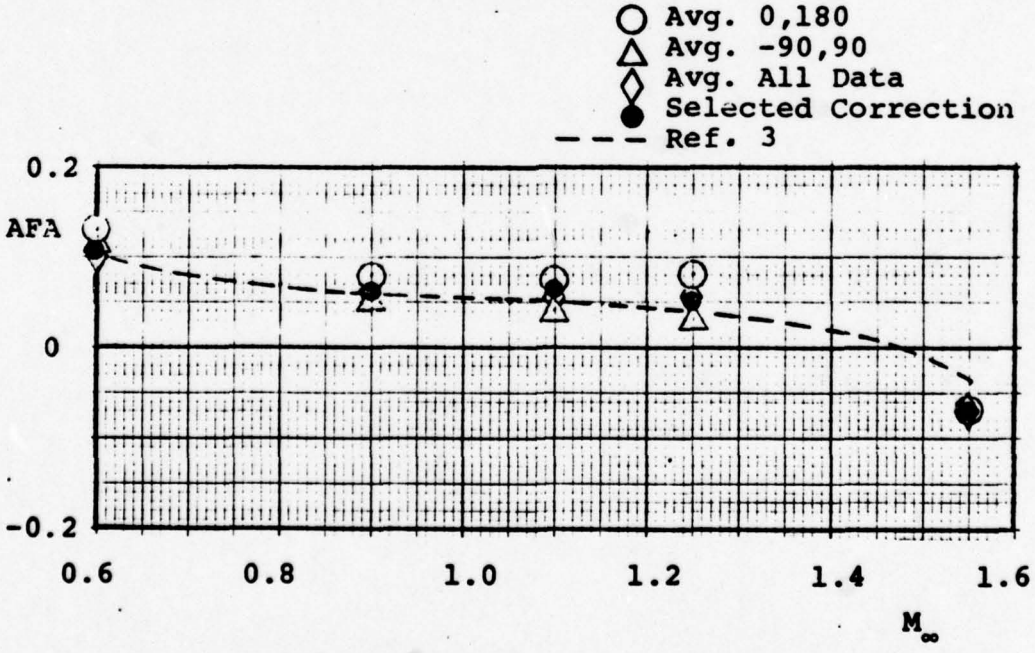

b. Selected Angular Corrections

Figure 7. Pitch Plane Angular Corrections

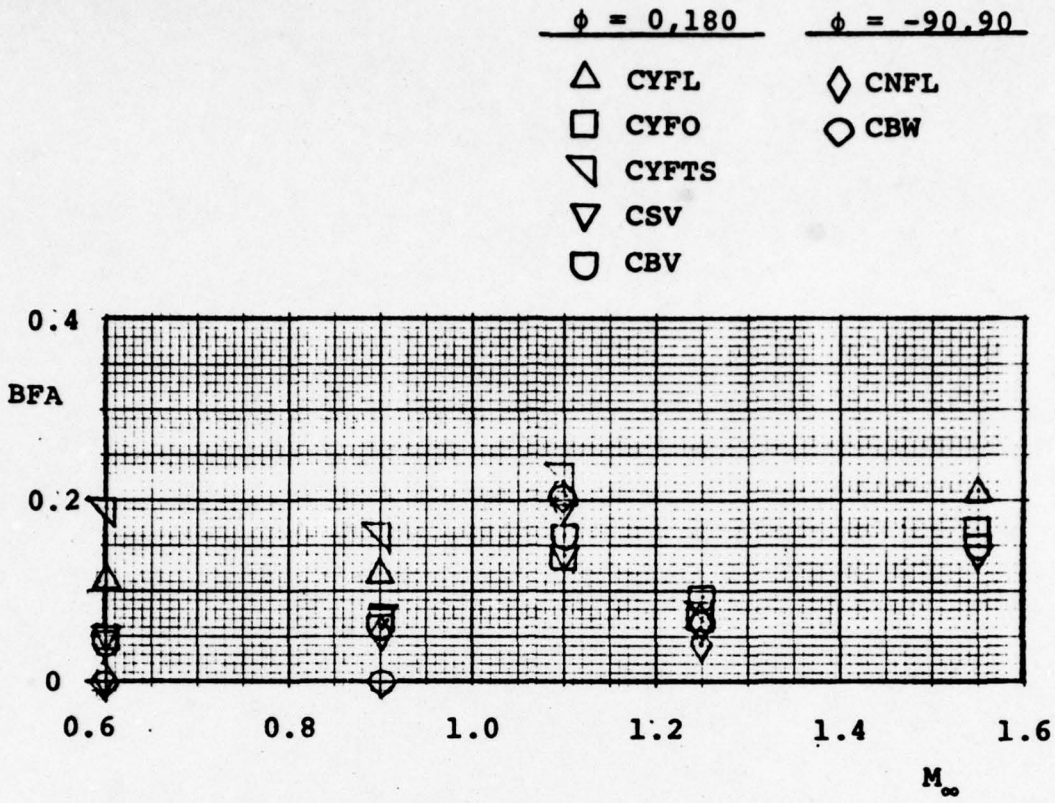

a. Angular Corrections Determined from 180-deg Opposed Balance Components

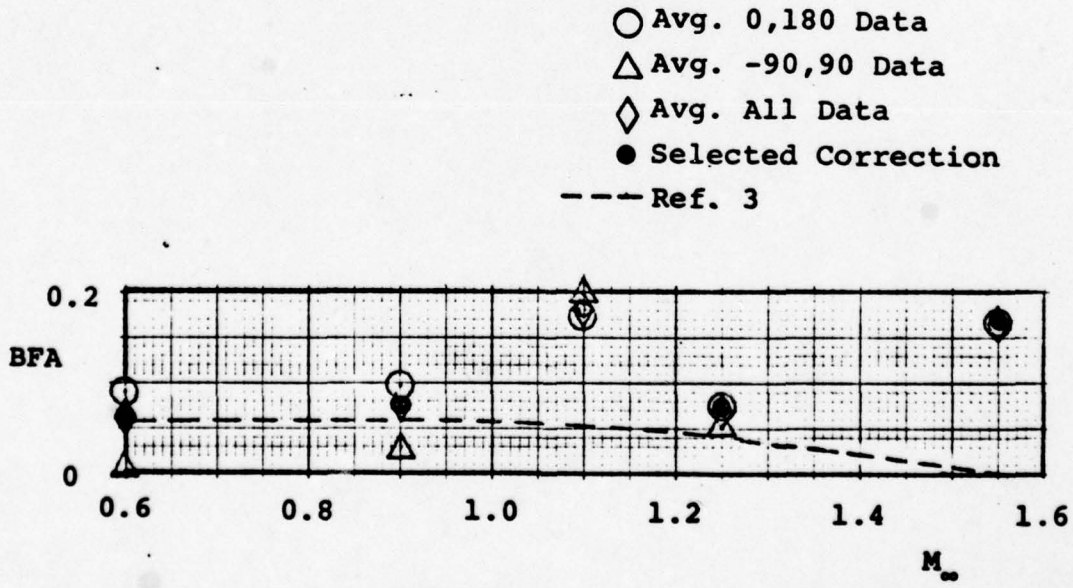

b. Selected Angular Corrections

Figure 8. Sideslip Plane Angular Corrections

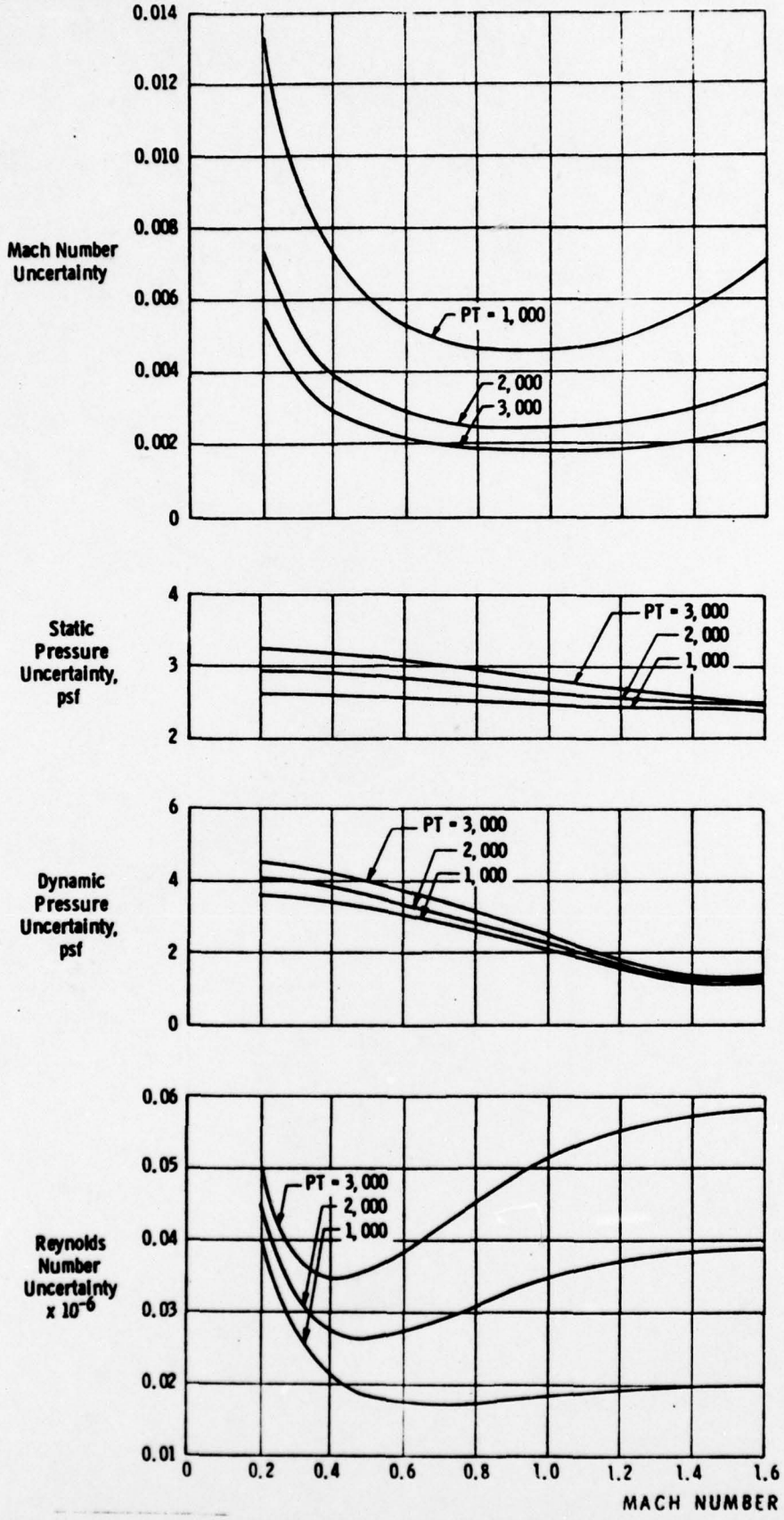

Figure 9. Estimated uncertainties in wind tunnel parameters.

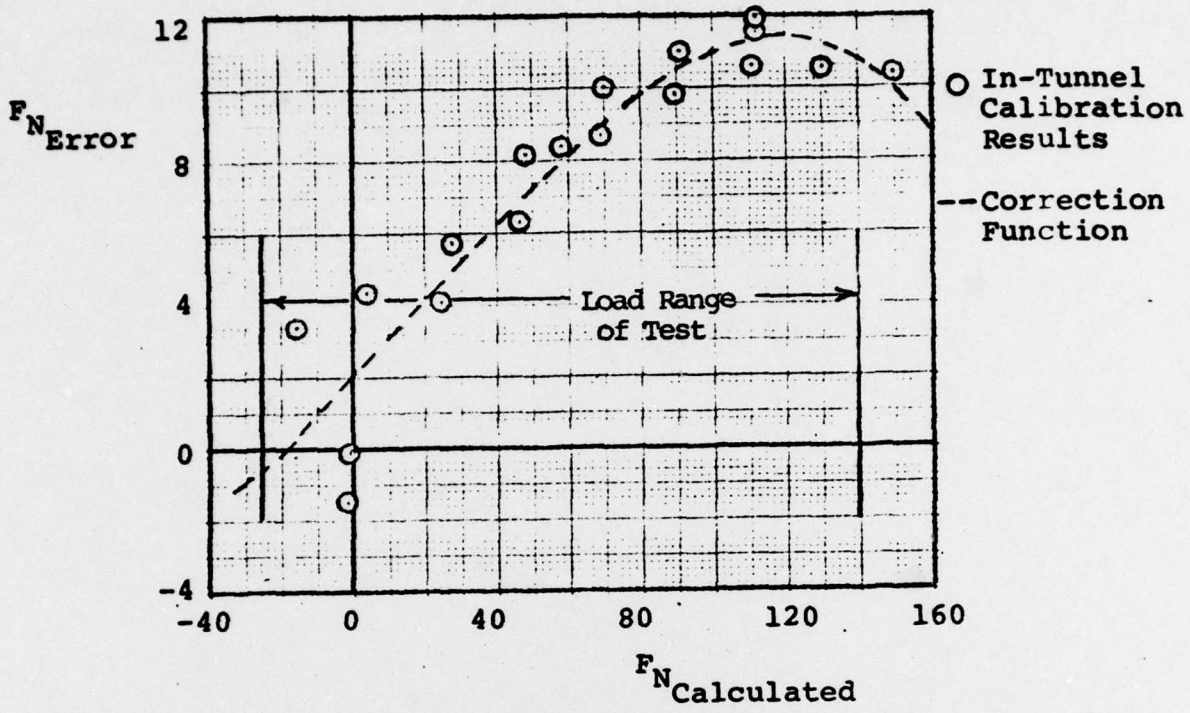

a. Increasing Wing Normal Force

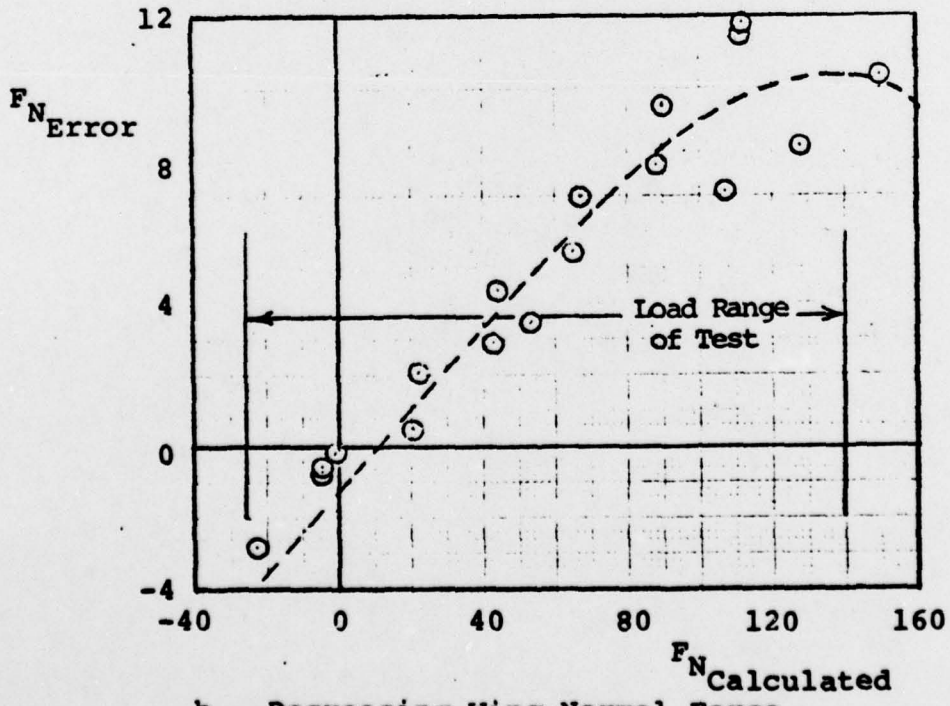

b. Decreasing Wing Normal Force

Figure 10. Wing Balance Normal Force Errors and Normal Force Correction Functions

Table 1. Model Attitude Schedules and Summary of Test Conditions

Flow Angularity Runs

α	β	ϕ	Mach Number 0.60	0.90	0.95	1.10	1.25	1.55
A	0	0	*3639/3696	3697	3698	3700/3701	3671/3705	3706
B	↓	↓				3702	3672	
A						3703	3673	
B		↓				3704	3674	
B	↓	180	3712	3713		3709	3675/3708	3707
0	C	90	3645/3717	3649/3714		3657	3667	
		-90	3716	3715		3718	3719	

*Part number

α/β Matrix Runs

M_∞	β	Angle of Attack, α: -8	-4	0	4
0.60	D	3640/3646	3641/3647	3645	3642/3648
0.90	↓	3650	3651	3649	3652
0.95		3654	3655	3653	3656
1.10		3658	3659	3657	3660
1.15		3664	3665	3663	3666
1.25	↓	3668	3669	3667	3670

Nominal Angle Schedules

A: α = -8,-6,-4,-2,0,2,4,6,8
B: α = 8,6,4,2,0,-2,-4,-6,-8
C: β = -6,-4,-2,0,2,4,6
D: β = -6,-4,0,4,6

Table 2. Sample of Data Tabulation

DATE. 1-19-79 PROJECT NO. P41T-31C
ARO, INC.
AEDC DIVISION
A SVERDRUP CORPORATION COMPANY
PROPULSION WIND TUNNEL
ARNOLD AIR FORCE STATION, TENNESSEE

PART	POINT	PROJECT	TEST	DATE	DAY	HR	MIN	SEC	MODE	DELP	PROC DATE	WIND-OFF	SET	
3639	4	P41T-81C	TF-519	11/15/78	319	1	20	32	7	336	01-19-79	135/	1	0

PROPULSION WIND TUNNEL
TRANSONIC 1ST

M	PT	P	Q	REX10-6	TT	TTR	H	PC	DP	WA	TPR	SHX10+3	PTI	PTE	CPR
0.601	1963.7	1538.8	388.6	3.007	109.9	569.6	8545.	1549.7	414.0	0.0	1.122	10.259	1750.0	1991.2	1.138

RATO	ATO	DELEIL	DELEOL	DELEINLR	DELEONLR	DELEIR	DELEOR
13091	-8.54	9.90	5.00	10.02	5.00	10.20	5.11

ALFI	PHII	ALFC	DALFL	DPSIL	DPHIL	DALFT	DPSIT	DPHIT	DALFLS	DPSILS	DPHILS	DALFRS	DPSIRS	DPHIRS
-7.99	-0.10	-8.12	-0.71	-0.01	0.01	0.09	-0.01	0.02	-0.16	-0.10	-0.00	-0.17	0.08	0.00

RALFI	RPHI	UNCORRECTED ANGLES	ALFAL	BETAL	ALFAT	BETAT	ALFALS	BETALS	ALFARS	BETARS
-7987	-10		-8.79	0.02	-8.70	0.03	-8.86	0.12	-8.87	-0.05

AFA	BFA	CORRECTED ANGLES	ALFAL	BETAL	ALFAT	BETAT	ALFALS	BETALS	ALFARS	BETARS
0.10	0.06		-8.69	0.09	-8.60	0.09	-8.76	0.19	-8.77	0.01

GAGE VOLTAGE

	1	2	3	4	5	6
ORBIT	-1.1334	-0.0980	1.1620	0.0575	0.6226	0.0243
ETANK	0.3255	-0.0406	1.0294	0.1622	-0.7480	-0.0847
SRBL	-0.7417	1.2052	0.6187	0.0097	-0.4270	0.7255
SRBR	-0.7500	-0.9514	0.5412	-0.0009	-0.3720	-0.5930
WING	-0.2045			-0.0532	-0.2271	
VERT	-0.2104			0.1385	-0.2346	
ELEVI	0.4856					
ELEVO	0.2798					

GAGE TOTAL LOAD

	1	2	3	4	5	6
ORBIT	-592.2	-9.6	88.47	31.7	191.1	4.3
ETANK	978.3	-9.1	72.71	21.1	-193.4	-34.5
SRBL	-405.4	238.9	16.09	-1.7	-150.0	145.1
SRBR	-437.1	-224.2	16.08	2.3	-161.5	-138.0
WING	-64.3			-35.0	-73.3	
VERT	-3.7			2.4	-4.8	
ELEVI	1.83					
ELEVO	0.59					

BALANCE GROSS LOADS

	FNG	FYG	FAG	MMG	MLG	MNG
ORBIT	-401.1	-5.2	98.5	-3262.4	31.7	-50.9
ETANK	-240.71	-5.0	73.1	397.5	21.1	-21.8
SRBL	-37.90	-14.7	16.1	-282.7	-1.7	-192.0
SRBR	-42.21	13.4	16.2	-299.3	2.3	181.1
WING	-19.93			-69.8	-35.0	
VERT	-1.77			-4.3	2.4	
ELEVI				1.93		
ELEVO				0.59		

STATIC TARES

	FNST	FYST	FAST	MMST	MLST	MNST
ORBIT	-200.0	-0.3	-30.0	-580.0	1.1	-1.0
ETANK	-87.0	-0.1	-13.4	538.4	-0.0	0.6
SRBL	-12.8	-0.0	-2.0	-29.7	-0.0	-0.0
SRBR	-12.9	-0.0	-2.0	-30.9	-0.0	-0.0
WING	-12.14			-25.4	-13.9	
VERT	-0.00			-0.0	0.0	
ELEVI				0.30		
ELEVO				0.10		

AERO LOADS AT BALANCE CENTER

	FN	FY	FA	MM	ML	MN
ORBIT	-201.04	-4.93	119.51	-2682.4	30.6	-49.9
ETANK	-153.67	-4.93	85.56	-141.0	21.1	-22.4
SRBL	-25.15	-14.67	19.17	-253.0	-1.7	-192.0
SRBR	-29.34	13.43	19.21	-268.4	2.3	181.2
WING	-7.79			-44.4	-21.0	
VERT	-1.77			-4.3	2.4	
ELEVI				1.53		
ELEVO				0.49		

	A	B	C
ORBIT	0.1528	-0.0015	0.9883
ETANK	0.1520	-0.0011	0.9884
SRBL	0.1548	-0.0009	0.9879
SRBR	0.1549	-0.0013	0.9879

P325	P302	P319	P413	P405	P1574	P1546	P1530	P1516	P1501	P2202	P2219
1449.5	1449.5	1441.1	1438.2	1440.4	1400.3	1399.4	1393.5	1388.3	1363.8	1381.4	1380.7

Table 2. Concluded

DATE. 1-19-79 PROJECT NO. P41T-31C
ARO, INC.
AEDC DIVISION
A SVERDRUP CORPORATION COMPANY
PROPULSION WIND TUNNEL
ARNOLD AIR FORCE STATION, TENNESSEE

PART	POINT	PROJECT	TEST	M	PT	P	Q	RX10-6	TT
3639	4	P41T-A1	TF519	0.601	1963.7	1538.8	388.5	3.007	110.

ALFAL	BETAL	CP325	CP302	CP319	CP413	CP405	CP1574	CP1546	CP1530	CP1516	CP1501	CP2202	CP2218
-6.69	0.09	-0.2297	-0.2299	-0.2514	-0.2589	-0.2533	-0.3564	-0.3586	-0.3737	-0.3974	-0.4502	-0.4049	-0.4069

BASE PRESSURE CORRECTIONS

CP1	CP2	CP3	CP4	CP5	CP6	CP7	CP9	CP10
-0.2299	-0.2561	-0.2514	-0.2297	-0.4049	-0.4049	-0.3792	-0.4069	-0.4059

CNBO	CABO	CLM30	CABT	CABLS	CYNBLS	CABRS	CYNBRS
0.0207	0.0383	-0.0113	0.0853	0.0356	-0.0069	0.0358	0.0069

LEFT SRB COEFFICIENTS

ALFAL	BETAL	ALFALS	BETALS	CNFLS	CAFLS	CALS	CYFLS	CLMF_S	CALLS	CYNFLS	CYN_S
-8.69	0.09	-8.76	0.19	-0.060	0.008	0.043	-0.035	0.017	-0.012	0.004	-0.003

RIGHT SRB COEFFICIENTS

ALFAL	BETAL	ALFARS	BETARS	CNFRS	CAFRS	CARS	CYFRS	CLMFRS	CALRS	CYNFRS	CYNRS
-8.69	0.09	-8.77	0.01	-0.070	0.009	0.044	0.032	0.022	0.014	-0.003	0.004

EXTERNAL TANK +(SRBL + SRBR) COEFFICIENTS

ALFAL	BETAL	ALFAT	BETAT	CNFTS	CAFTS	CATS	CYFTS	CLMTS	CALFTS	CYNFTS	CYNTS
-8.69	0.09	-8.60	0.09	-0.368	0.030	0.207	-0.012	0.054	0.002	0.000	0.000

EXTERNAL TANK COEFFICIENTS

ALFAL	BETAL	ALFAT	BETAT	CNFT	CAFT	CYFT	CLMFT	CALFT	CYNFT
-8.69	0.09	-8.60	0.09	-0.237	0.035	-0.009	0.015	-0.000	-0.001

LAUNCH VEHICLE COEFFICIENTS

ALFAL	BETAL	CNFL	CAFL	CAL	CYFLI	CLMFLI	CALFL	CYNFL	CYN_I	CNL
-8.69	0.09	-0.501	0.093	0.283	-0.012	0.150	-0.000	0.003	0.003	-0.481

ORBITER COEFFICIENTS

ALFAL	BETAL	CNFO	CAFO	CYFO	CLMFO	CALFO	CYNFO	DELEIR	DELEOR
-8.69	0.09	-0.134	0.038	-0.000	0.106	-0.002	0.003	10.20	5.11

ALFAL	BETAL	CNW	CBW	CTW	CSVT	CBVT	CTVT	CHEI	CHEO
-8.69	0.09	-0.019	-0.005	-0.008	-0.027	-0.020	0.008	0.026	0.008

Table 3. Data Tabulation Nomenclature

Tunnel Parameters

CPR	Compressor pressure ratio
DATE	Date of data processing
DAY	Day (of year) of data acquisition
DELP	Primary input deletion and selection code
DP	Differential pressure, (PT-PC), psf
H	Pressure altitude, ft
HR	Hour of data acquisition
M	Free-stream Mach number
MIN	Minute of data acquisition
MODE	Data acquisition mode
P	Free-stream static pressure, psfa
PART	Part number (a data subset containing variations of only one independent parameter)
POINT	Point number (a single record of all test parameters)
PROC DATE	Date of data processing
PROJECT	AEDC project number
PT	Free-stream total pressure, psfa
PTE	Compressor exit pressure, psfa
PTI	Compressor inlet pressure, psfa
Q	Free-stream dynamic pressure, psf
Rex10-6	Free-stream unit Reynolds number, per foot
SEC	Second of data acquisition
SET	Constant set used

Table 3. Continued

SHX10+3	Tunnel specific humidity, lb/lb
TEST	PWT test number
TPR	Tunnel pressure ratio
TT	Free-stream stagnation temperature, °F
TTR	Free-stream stagnation temperature, °R
WA	Test section wall angle, deg
WINDOFF	Wind-off part and point number

Test Parameters

A	Trigonometric function used in determining model static tares
AFA	Angularity correction in the tunnel pitch plane, positive up, deg

The following angles are identified by Line as uncorrected model angles (without angularity correction) and as corrected model angles (angularity correction included).

ALFAL	Launch vehicle angle of attack, deg
ALFALS	Left SRB angle of attack, deg
ALFARS	Right SRB angle of attack, deg
ALFAT	External tank angle of attack, deg
BETAL	Launch vehicle sideslip angle, deg
BETALS	Left SRB sideslip angle, deg
BETARS	Right SRB sideslip angle, deg
BETAT	External tank sideslip angle, deg
ALFC	Effective sting pitch angle, deg
ALFI	Indicated sting pitch angle, deg
ATD	ET angle of attack as measured by a strain gage pendulum, deg

Table 3. Continued

B	Trigonometric function used in calculation of model static tares
BFA	Angularity correction in the tunnel cross flow plane, positive from right to left looking upstream, deg
C	Trigonometric function used in calculation of model static tares
CP302-CP2218	(not inclusive) Base pressure coefficients determined from pressures measured on model components, Pn-P/q
DALFL	Launch vehicle sting and balance deflection in the pitch plane, deg
DALFLS	Left SRB balance deflection in the pitch plane, deg
DALFRS	Right SRB balance deflection in the pitch plane, deg
DALFT	ET balance deflection in the pitch plane, deg
DELEIL	Left hand inboard elevon nominal deflection angle, deg
DELEINLR	Right hand inboard elevon deflection angle in an unloaded condition, deg
DELEIR	Right hand inboard elevon deflection angle including deflections resulting from aero loading, deg
DELEOL	Left hand outboard elevon nominal deflection angle, deg
DELEONLR	Right hand outboard elevon deflection angle in an unloaded condition, deg
DELEOR	Right hand outboard elevon nominal deflection angle, deg
DPHIL	Roll deflection of the launch vehicle sting and balance, deg
DPHILS	Roll deflection of the left SRB balance, deg
DPHIRS	Roll deflection of the right SRB balance, deg
DPHIT	Roll deflection of the ET balance, deg

Table 3. Continued

DPSIL	Yaw deflection of the launch vehicle sting and balance, deg
DPSILS	Yaw deflection of the left SRB balance, deg
DPSIRS	Yaw deflection of the right SRB balance, deg
DPSIT	Yaw deflection of the ET balance, deg

Balance Identification

ELEVI	Inboard elevon hinge moment balance
ELEVO	Outboard elevon hinge moment balance
ETANK	External tank balance measuring combined loads of ET and SRB's
ORBIT	Orbiter balance measuring total launch vehicle loads
SRBL	Left solid rocket booster balance
SRBR	Right solid rocket booster balance
VERT	Vertical tail balance
WING	Left hand wing balance
FA	Model aerodynamic axial force, lb
FAG	Total axial force on balance (including static tare force), lb
FAST	Axial force static tare, lb
FN	Model aerodynamic normal force, lb
FNG	Total normal force on balance (including static tare force), lb
FNST	Normal force static tare, lb
FY	Model aerodynamic side force, lb
FYG	Total side force on balance (including static tare force), lb
FYST	Side force static tare, lb
GAGE TOTAL LOAD	Balance gage total loads, lb or in.-lb

Table 3. Continued

GAGE VOLTAGE	Balance gage total loads, volts
ML	Model aerodynamic rolling moment about the model reference point, in.-lb
MLG	Total rolling moment measured by balance (including static tare loads), in.-lb
MLST	Rolling moment static tare, in.-lb
MM	Model aerodynamic pitching moment about the model reference point, in.-lb
MMG	Total pitching moment measured by balance (including static tare loads), in.-lb
MMST	Pitching moment static tare, in.-lb
MN	Model aerodynamic yawing moment about the model reference point, in.-lb
MNG	Total yawing moment measured by balance (including static tare loads), in.-lb
MNST	Yawing moment static tare, in.-lb
PHII	Indicated sting roll angle, deg
P302-P2218 (not inclusive)	Model component base pressures, psfa (Fig. 4)
RALFI	Sting pitch indicator instrument reading, counts
RATD	Strain gage pendulum angle of attack instrument reading, counts
RPHI	Sting roll angle instrument reading, counts
1-6	Individual balance gage loadings

Base Pressure Corrections

CABO	Orbiter base axial force coefficient, body axes, force/$Q(S_{REF})$
CABLS	Left SRB base axial force coefficient, body axes, force/$Q(S_{REF})$
CABRS	Right SRB base axial force coefficient, body axes, force/$Q(S_{REF})$

Table 3. Continued

CABT	ET base axial force coefficient, body axes, force/$Q(S_{REF})$
CLMBO	Orbiter base pitching-moment coefficient, body axes, moment/$Q(S_{REF})(\ell_{REF})$
CNBO	Orbiter base normal force coefficient, body axes, force/$Q(S_{REF})$
CYNBLS	Left SRB base yawing moment coefficient, body axes, moment/$Q(S_{REF})(\ell_{REF})$
CYNBRS	Right SRB base yawing moment coefficient, body axes, moment/$Q(S_{REF})(\ell_{REF})$
CP1-CP10	(not inclusive) Base pressure area weighted coefficients

Left SRB Coefficients

CAFLS	Forebody axial force coefficient, body axes, force/$Q(S_{REF})$
CALS	Measured axial force coefficient, body axes, force/$Q(S_{REF})$
CBLLS	Measured rolling moment coefficient, body axes, moment/$Q(S_{REF})(\ell_{REF})$
CLMFLS	Forebody pitching-moment coefficient, body axes, moment/$Q(S_{REF})(\ell_{REF})$
CNFLS	Forebody normal force coefficient, body axes, force/$Q(S_{REF})$
CYFLS	Forebody side force coefficient, body axes, force/$Q(S_{REF})$
CYNFLS	Forebody yawing moment coefficient, moment/$Q(S_{REF})(\ell_{REF})$
CYNLS	Measured yawing moment coefficient, moment/$Q(S_{REF})(\ell_{REF})$

Right SRB Coefficients

CAFRS	Forebody axial force coefficient, body axes, force/$Q(S_{REF})$

Table 3. Continued

CARS	Measured axial force coefficient, body axes, force/$Q(S_{REF})$
CBLRS	Measured rolling moment coefficient, body axes, moment/$Q(S_{REF})(\ell_{REF})$
CLMFRS	Forebody pitching-moment coefficient, body axes, moment/$Q(S_{REF})(\ell_{REF})$
CNFRS	Forebody normal force coefficient, body axes, force/$Q(S_{REF})$
CYFRS	Forebody side force coefficient, body axes, force/$Q(S_{REF})$
CYNFRS	Forebody yawing moment coefficient, moment/$Q(S_{REF})(\ell_{REF})$
CYNRS	Measured yawing moment coefficient, moment/$Q(S_{REF})(\ell_{REF})$

External Tank + (SRBL + SRBP) Coefficients

CAFTS	Forebody and force coefficient, body axes, force/$Q(S_{REF})$
CATS	Measured axial force coefficient, body axes, force/$Q(S_{REF})$
CBLFTS	Measured rolling moment coefficient, body axes, moment/$Q(S_{REF})(\ell_{REF})$
CLMTS	Forebody pitching-moment coefficient, body axes, moment/$Q(S_{REF})(\ell_{REF})$
CNFTS	Forebody normal force coefficient, body axes, force/$Q(S_{REF})$
CYFTS	Forebody side force coefficient, body axes, force/$Q(S_{REF})$
CYNFTS	Forebody yawing moment coefficient, moment/$Q(S_{REF})(\ell_{REF})$
CYNTS	Measured yawing moment coefficient, moment/$Q(S_{REF})(\ell_{REF})$

Table 3. Continued

External Tank Coefficients

CAFT	Forebody axial force coefficient, body axes, force/$Q(S_{REF})$
CBLFT	Forebody rolling moment coefficient, body axes, moment/$Q(S_{REF})(\ell_{REF})$
CLMFT	Forebody pitching-moment coefficient, body axes, moment/$Q(S_{REF})(\ell_{REF})$
CNFT	Forebody normal force coefficient, body axes, force/$Q(S_{REF})$
CYFT	Forebody side force coefficient, body axes, force/$Q(S_{REF})$
CYNFT	Forebody yawing moment coefficient, moment/$Q(S_{REF})(\ell_{REF})$

Launch Vehicle Coefficients

CAFL	Forebody axial force coefficient, body axes, force/$Q(S_{REF})$
CAL	Measured axial force coefficient, body axes, force/$Q(S_{REF})$
CBLFL	Forebody rolling moment coefficient, body axes, moment/$Q(S_{REF})(\ell_{REF})$
CLMFL	Forebody pitching-moment coefficient, body axes, moment/$Q(S_{REF})(\ell_{REF})$
CNFL	Forebody normal force coefficient, body axes, force/$Q(S_{REF})$
CNL	Measured normal force coefficient, body axes, force/$Q(S_{REF})$
CYFL	Forebody side force coefficient, body axes, force/$Q(S_{REF})$
CYNFL	Forebody yawing moment coefficient, moment/$Q(S_{REF})(\ell_{REF})$
CYNL	Measured yawing moment coefficient, moment/$Q(S_{REF})(\ell_{REF})$

Table 3. Concluded

Orbiter Coefficients

CAFO	Orbiter axial force coefficient, body axes, force/$Q(S_{REF})$
CBLFO	Measured rolling moment coefficient, body axes, moment/$Q(S_{REF})(\ell_{REF})$
CLMFO	Forebody pitching-moment coefficient, body axes, moment/$Q(S_{REF})(\ell_{REF})$
CNFO	Forebody normal force coefficient, body axes, force/$Q(S_{REF})$
CYFO	Forebody side force coefficient, body axes, force/$Q(S_{REF})$
CYNFO	Forebody yawing moment coefficient, moment/$Q(S_{REF})(\ell_{REF})$

Vertical Tail Coefficients

CBV	Bending moment coefficient, moment/$Q(S_{REF})(\ell_{REF})$
CSV	Side force coefficient, force/$Q(S_{REF})$
CTV	Torsional moment coefficient, moment/$Q(S_{REF})(\ell_{REF})$

Wing Coefficients

CBW	Bending moment coefficient of the wing, moment/$Q(S_{REF})b$
CNW	Normal force coefficient of the wing, force/$Q(S_{REF})$
CTW	Torsional moment coefficient of the wing, moment/$Q(S_{REF})\bar{c}$

Elevon Coefficients

CHEI	Inboard elevon hinge moment coefficient, moment/$Q(S_{REF})(\ell_{REF})$
CHEO	Outboard elevon hinge moment coefficient, moment/$Q(S_{REF})(\ell_{REF})$